Gating Kinetics of Single Large-Conductance Ca^{2+}-activated K^+ Channels in High Ca^{2+} Suggest a Two-Tiered Allosteric Gating Mechanism✪

Brad S. Rothberg and Karl L. Magleby

From the Department of Physiology and Biophysics, University of Miami School of Medicine, Miami, Florida 33101-6430

abstract The Ca^{2+}-dependent gating mechanism of large-conductance calcium-activated K^+ (BK) channels from cultured rat skeletal muscle was examined from low (4 μM) to high (1,024 μM) intracellular concentrations of calcium (Ca^{2+}_i) using single-channel recording. Open probability (P_o) increased with increasing Ca^{2+}_i ($K_{0.5}$ 11.2 ± 0.3 μM at +30 mV, Hill coefficient of 3.5 ± 0.3), reaching a maximum of ~0.97 for $Ca^{2+}_i \sim 100$ μM. Increasing Ca^{2+}_i further to 1,024 μM had little additional effect on either P_o or the single-channel kinetics. The channels gated among at least three to four open and four to five closed states at high levels of Ca^{2+}_i (>100 μM), compared with three to four open and five to seven closed states at lower Ca^{2+}_i. The ability of kinetic schemes to account for the single-channel kinetics was examined with simultaneous maximum likelihood fitting of two-dimensional (2-D) dwell-time distributions obtained from low to high Ca^{2+}_i. Kinetic schemes drawn from the 10-state Monod-Wyman-Changeux model could not describe the dwell-time distributions from low to high Ca^{2+}_i. Kinetic schemes drawn from Eigen's general model for a ligand-activated tetrameric protein could approximate the dwell-time distributions but not the dependency (correlations) between adjacent intervals at high Ca^{2+}_i. However, models drawn from a general 50 state two-tiered scheme, in which there were 25 closed states on the upper tier and 25 open states on the lower tier, could approximate both the dwell-time distributions and the dependency from low to high Ca^{2+}_i. In the two-tiered model, the BK channel can open directly from each closed state, and a minimum of five open and five closed states are available for gating at any given Ca^{2+}_i. A model that assumed that the apparent Ca^{2+}-binding steps can reach a maximum rate at high Ca^{2+}_i could also approximate the gating from low to high Ca^{2+}_i. The considered models can serve as working hypotheses for the gating of BK channels.

key words: BK channel • K_{Ca} channel • Monod-Wyman-Changeux • Eigen • Markov

introduction

Large-conductance Ca^{2+}-activated K^+ (BK)[1] channels, which are activated by micromolar concentrations of intracellular Ca^{2+} (Ca^{2+}_i) and by depolarization (Barrett et al., 1982) are present in a wide variety of tissues (reviewed by Rudy, 1988; Marty, 1989; McManus, 1991; Latorre, 1994; Conly, 1996). Activated BK channels reduce membrane excitability by allowing K^+ efflux through their opened pores, which drives the membrane potential more negative. Hence, BK channels form a link in a negative feed-back loop that decreases excitability in response to both increased Ca^{2+}_i and depolarization.

Information about the gating mechanism of BK channels has accumulated from kinetic studies on native and heterologously expressed channels. BK channels are homotetramers, formed from four alpha subunits (Shen et al., 1994), with one or more Ca^{2+}-binding sites per subunit (Schreiber and Salkoff, 1997). BK channels typically display a steep relation between Ca^{2+}_i and open probability, P_o, with Hill coefficients usually in the range of 2–4 (Barrett et al. 1982; Wong et al., 1982; Golowasch et al., 1986; Oberhauser et al., 1988; Reinhart et al., 1989; McManus and Magleby, 1991; Art et al., 1995; DiChiara and Reinhart, 1995; Cui et al., 1997). Hill coefficients >1 suggest a cooperative action of Ca^{2+} on P_o, and are often associated with allosteric modulation of activity (Colquhoun 1973; Fersht 1985).

Models drawn from the Monod-Wyman-Changeux (MWC) model (Monod et al., 1965) describing the transitions of tetrameric allosteric proteins have often been used to describe the Ca^{2+}-dependent gating of BK channels. For example, McManus and Magleby (1991) found that a model with three open and five closed states drawn from the MWC model could account for many of the basic features of the Ca^{2+} dependence of the single-channel gating kinetics from low to intermediate levels of activity, and Cox et al. (1997b) found that the full 10-state MWC model (and also an extended 12-state model) could account for macroscopic conductance–voltage relations over a wide range of Ca^{2+}_i.

Address correspondence to Dr. Karl L. Magleby, Dept. of Physiology and Biophysics (R-430), University of Miami School of Medicine, Miami, FL 33101-6430. Fax: 305-243-6898; E-mail: kmagleby@miami.edu

✪The online version of this article contains supplemental material.

[1]*Abbreviations used in this paper:* 1-D, 1-dimensional; BK channel, large-conductance calcium-activated K^+ channel; MWC, Monod-Wyman-Changeux; NLR_{1000}, normalized likelihood ratio.

Despite these successes, MWC-type models appear too simple to account for certain details of BK channel gating. Cox et al. (1997b) found that such a model would not account for the details of the macroscopic activation and deactivation kinetics at large positive or negative potentials, and a number of studies have suggested that closed states in addition to those in the MWC model may contribute to the gating (Wu et al., 1995; Cox et al. 1997b). For example, Rothberg and Magleby (1998) found that gating mechanisms drawn from the MWC model underpredicted the numbers of brief closed intervals (flickers) adjacent to the various open intervals. Single-channel analysis then suggested that there were additional closed states, either intermediate (in the activation pathway) or secondary (beyond the activation pathway) that contributed to the generation of the flickers.

We now test further whether the above extensions of the MWC model are consistent with the underlying gating mechanism. Our approach is to examine the activity of single BK channels from low (4 μM) to very high (~1 mM) intracellular concentrations of Ca^{2+} (Ca^{2+}_i). By driving the channel toward its fully liganded states, we estimated the numbers of open and closed states involved in the gating at high Ca^{2+}_i, and through analysis of two-dimensional dwell-time distributions and dependency plots, we determined the minimum number of independent transition pathways connecting the fully liganded open and closed states.

We found that at high Ca^{2+}_i, the BK channel gates among three to four open and four to five closed states, with two or more effective transition pathways (gateway states) connecting the open and closed states. Neither the general model of Eigen (1968) nor the 55-state extension of Eigen's model by Cox et al. (1997b) appear consistent with these findings for the gating at high Ca^{2+}_i. Extensions of Eigen's model to a two-tiered gating mechanism, in which the upper tier was comprised of closed states and the lower tier was comprised of open states, provided a model that would allow gating in the necessary numbers of open and closed states at high Ca^{2+}_i, together with the required multiple transition pathways between open and closed states. In the two-tiered model, each of the closed conformations of the channel can undergo a direct (possibly concerted) transition to an open conformation. Models drawn from the general two-tiered model could describe the single-channel kinetics from low to high Ca^{2+}_i. Since the general two-tiered model (and simple extensions of this model) contain previous models that have been used to account for gating under more limited conditions (McManus and Magleby, 1991; Rothberg and Magleby, 1998), it can serve to unify descriptions of gating. A simpler model that assumed the Ca^{2+}-dependent transition rates approached a maximum in high Ca^{2+}_i could also approximate many features of the single-channel kinetics from low to high Ca^{2+}_i. The considered models can serve as working hypotheses to further study the gating mechanisms of BK channels.

methods

Preparation

Currents flowing through single BK channels in patches of surface membrane excised from primary cultures of rat skeletal muscle (myotubes) were recorded using the patch clamp technique (Hamill et al., 1981). Cultures of rat myotubes were prepared from fetal skeletal muscle as described previously (Barrett et al., 1982; Bello and Magleby, 1998). All recordings were made at +30 mV using the excised inside-out configuration of the patch clamp technique in which the intracellular surface of the patch was exposed to the bathing solution. Analysis was restricted to patches containing a single BK channel. Single-channel patches were identified by observing openings to only a single open channel conductance level during several minutes of recording in which the P_o was >0.4. Experiments were performed at room temperature (22–24°C). Data are presented as mean ± SD.

Solutions

The solutions bathing both sides of the membrane contained 150 mM KCl and 5 mM TES (*N*-tris(hydroxymethyl)methyl-2-aminoethane sulfonate) pH buffer, with the pH of the solutions adjusted to 7.0. Contaminant Ca^{2+}_i was determined by atomic absorption spectrometry. The solution at the intracellular side of the membrane also contained added Ca^{2+} (as $CaCl_2$), to bring the Ca^{2+} concentration at the intracellular surface (Ca^{2+}_i) to the indicated levels. (The solutions did not contain Ca^{2+} buffers.) No Ca^{2+} was added to the extracellular (pipette) solution. Solutions were changed through the use of a microchamber (Barrett et al., 1982).

Recording and Measuring Interval Durations and Identifying Normal Activity

Single-channel currents were recorded on a digital data recorder (DC-37 kHz; Instrutech Corp.), low-pass filtered with a four-pole Bessel filter to give a final effective filtering of 6–10 kHz (−3 dB), and sampled by computer at a rate of 125–200 kHz. The effective filtering is expressed in terms of dead time, which is the duration of an underlying interval before filtering that would just reach 50% of the single-channel current amplitude with filtering (Colquhoun and Sigworth, 1995). Five channels in which stable single-channel data were obtained over a wide range of Ca^{2+}_i were analyzed in detail. The channels and their dead times were: B04, 16 μs; B06 and B16, 28.5 μs; B12, 22.9 μs, and B14, 17.9 μs. The sampled currents were analyzed using custom programs written in the laboratory. The methods used to set the level of filtering to exclude false events that could arise from noise, measure interval durations with half-amplitude threshold analysis, test for stability, and identify activity in the various modes using stability plots, have been described previously, including the precautions taken to prevent artifacts in the analysis (McManus et al., 1987; McManus and Magleby, 1988, 1989; Magleby, 1992).

Restriction of Analysis to Activity in the Normal Mode

The analysis in the present study was restricted to channel activity in the normal mode, which typically involves ~96% of the detected intervals (McManus and Magleby, 1988). Activity in modes

other than normal, including the low activity mode and transitions to isolated long shut intervals, were removed before analysis. The low activity mode is readily distinguished from normal activity over the range of low to high Ca^{2+}_i, as detailed in Rothberg et al. (1996). The isolated long shut intervals are also readily identified at high Ca^{2+}_i, and appear to contribute an insignificant number of the long shut intervals at lower Ca^{2+}_i (Rothberg et al., 1996). The mean frequency and duration of the isolated long shut intervals are Ca^{2+} independent, indicating that isolated long shut intervals do not arise from discrete Ca^{2+} block (Rothberg et al., 1996). In spite of their low frequency, appreciable time can be spent in the isolated long shut intervals at high Ca^{2+}_i because most of the other closed intervals are so brief. For higher Ca^{2+}_is that give P_os > 0.8, BK channels can spend $>30\%$ of their time in the low activity mode that has a P_o of ~ 0.001 (Rothberg et al., 1996). Because of the potential effects of the low activity mode and isolated long shut intervals on the single-channel record, it is essential to identify and exclude these (and other modes), as we have done, when studying normal activity over a wide range of Ca^{2+}_i.

Log Binning and Plotting of One- and Two-Dimensional Dwell-Time Distributions

Both one- (1-D) and two-dimensional (2-D) dwell-time distributions were analyzed. The 1-D distributions of open and closed interval durations were log-binned as described previously (McManus et al., 1987) at a resolution of 25 bins per log unit for fitting with mixtures (sums) of exponential components. Details of estimating the numbers of significant exponential components are in McManus and Magleby (1988), including the use of the likelihood ratio test for significance. The 2-D distributions of adjacent open–closed interval pairs (Fredkin et al., 1985) were log-binned at a resolution of 10 bins per log unit, as described previously (Magleby and Weiss, 1990b; Rothberg et al., 1997). The 2-D distributions were fitted with mixtures (sums) of 2-D exponential components to estimate the numbers of underlying 2-D exponential components, and hence the minimum number of kinetic states, as detailed in Rothberg et al. (1997).

With filtering, detected intervals with durations less than about twice the dead time are narrowed (McManus et al., 1987; Colquhoun and Sigworth, 1995). For the plotting of 2-D dwell-time distributions, the plotted intervals have not been corrected for this narrowing. For the fitting of kinetic models using 2-D dwell-time distributions, the measured durations of these intervals were corrected to their estimated true durations before binning and fitting, using the numerical method in Colquhoun and Sigworth (1995). Even with correction, the data were typically fit starting at ~ 1.5 dead times for two reasons: (a) intervals whose underlying (true) durations are less than the dead time can be detected when data are filtered, placing an excess of intervals in the first few bins (Magleby and Weiss, 1990a), and (b) intervals that are undetected due to filtering (missed events) can introduce extra (phantom) components with time constants typically less than one-half the dead time (Roux and Sauve, 1985; Blatz and Magleby, 1986; Hawkes et al., 1992; Magleby and Weiss, 1990a), which can also add excess intervals to the first few bins. Depending on the gating mechanism, noise, and filtering, the excess intervals arising from either phenomena can lead to the detection of excess brief exponential components if the fitting includes intervals less than ~ 1.5–2 dead times.

Dependency Plots

Dependency plots were constructed from the 2-D dwell-time distributions as detailed in Magleby and Song (1992) and Rothberg and Magleby (1998). In brief, the dependency for each bin of open–closed interval pairs with mean durations t_O and t_C is:

$$\text{dependency}(t_O,t_C) = \frac{N_{Obs}(t_O,t_C) - N_{Ind}(t_O,t_C)}{N_{Ind}(t_O,t_C)}, \quad (1)$$

where $N_{Obs}(t_O,t_C)$ is the experimentally observed number of interval pairs in bin (t_O,t_C), and $N_{Ind}(t_O,t_C)$ is the calculated number of interval pairs in bin (t_O,t_C) if adjacent open and closed intervals pair independently (at random). The method of calculating expected frequencies for observations that are independent (contingency tables) is a common statistical procedure (compare Mendenhall et al., 1990). The expected number of interval pairs in bin (t_O,t_C) for independent pairing is:

$$N_{Ind}(t_O,t_C) = P(t_O) \times P(t_C), \quad (2)$$

where $P(t_O)$ is the probability of an open interval falling in the row of bins with a mean open duration of t_O, and $P(t_C)$ is the probability of a closed interval falling in the column of bins with a mean closed duration of t_C. $P(t_O)$ is given by the number of open intervals in row t_O divided by the total number of open intervals in all rows, and $P(t_C)$ is given by the number of closed intervals in column t_C divided by the total number of closed intervals in all columns. Since open and closed intervals are paired, the total number of open intervals is equal to the total number of closed intervals. Each open and closed interval forms two pairs: one with the preceding interval and one with the following interval. Hence, the number of interval pairs in a 2-D dwell-time distribution is equal to the number of open plus closed intervals minus one.

Estimating the Most Likely Rate Constants for Kinetic Schemes

The most likely rate constants for the examined kinetic schemes were estimated from the simultaneous fitting of the 2-D dwell-time distributions obtained at six different Ca^{2+}_i using the iterative maximum likelihood fitting procedure described in Rothberg and Magleby (1998) with Q-matrix methods to calculate the predicted 2-D dwell-time distributions (Fredkin et al., 1985; Colquhoun and Hawkes, 1995b). Corrections for missed events were applied during the fitting using the method described in Crouzy and Sigworth (1990). Since the gating of native BK channels in rat skeletal muscle appears consistent with microscopic reversibility (Song and Magleby, 1994), microscopic reversibility was maintained during the fitting.

The number of underlying 2-D exponential components that sum to form a 2-D dwell-time distribution is given by the product of the numbers of open and closed states (Fredkin et al., 1985; Rothberg et al., 1997). Thus, a single 2-D dwell-time distribution fitted with, for example, three open and five closed 2-D exponential components can potentially define 22 parameters: three open and five closed time constants and the volumes of 14 of 15 (3×5) underlying 2-D components. One of the volumes is not free since the volumes must sum to 1.0. Simultaneous fitting of three to six 2-D dwell-time distributions obtained at different Ca^{2+}_i further increased the information available to estimate the fixed number of rate constants that defined the models. In spite of all this information, rate constants can remain ill-defined in complex models (Fredkin et al., 1985; Bauer et al., 1987), which is why the analysis in this paper has been restricted to models with the fewest numbers of states that can approximate the examined kinetic features of the data. Rather than estimating the uncertainty in the rate constants for any single experiment, the uncertainty was estimated by comparing rate constants obtained from fitting data from different channels.

For a given model and rate constants, the equilibrium occu-

pancies of the states could be calculated as described in Colquhoun and Hawkes (1995b). The frequencies of entry into each state could then be calculated by dividing the equilibrium occupancy of a state by its mean lifetime.

Evaluating Kinetic Schemes

Normalized likelihood ratios (NLR_{1000}) have been used to indicate how well any given kinetic scheme describes the 2-D dwell-time distributions when compared with a theoretical best description of the data. Normalization corrects for the differences in numbers of interval pairs among experiments so that comparisons can be made among channels. The normalized likelihood ratio per 1,000 interval pairs is defined as

$$NLR_{1000} = \exp[(\ln S - \ln T)(1,000/n)], \quad (3)$$

where $\ln S$ is the natural logarithm of the maximum likelihood estimate for the observed 2-D dwell-time distributions given the kinetic scheme, $\ln T$ is the natural logarithm of the likelihood of the theoretical best description of the observed distributions, and n is the total number of fitted interval pairs (events) in the observed dwell-time distributions (McManus and Magleby, 1991; Weiss and Magleby, 1992; Rothberg and Magleby, 1998).

The NLR gives a measure of how well different kinetic schemes describe the distributions, but it cannot be used to directly rank schemes since no penalty is applied for the numbers of free parameters. To overcome this difficulty, models were ranked using an information criteria approach (Akaike, 1974; Horn, 1987), which has the limitation that the significance level is not known. If

$$\log_e(m_g/m_f) > (k_g - k_f), \quad (4)$$

then model g is ranked above model f, where m_g and m_f are the maximum likelihood estimates for models g and f, and k_g and k_f are the number of free parameters for each scheme. We also compared the Akaike rankings to those of the Schwarz (1978) criterion and found that the Akaike rankings for different schemes were more consistent among channels and also were in better agreement with rankings based on the visual perception of the ability of models to describe major features of the data.

Estimating the Theoretical Best Descriptions of the 2-D Dwell-Time Distributions

To evaluate models, it was useful to have an estimate of the theoretical best descriptions of the dwell-time distributions for comparison to the distributions predicted by the various examined gating mechanisms. For gating consistent with a discrete state Markov process (the rate constants remain constant in time for constant experimental conditions), as appears to be the case for BK channels (McManus and Magleby, 1989; Petracci et al., 1991), the log likelihood for a theoretical best description of the 2-D dwell-time distribution could be obtained by fitting the distribution with an uncoupled (generic) scheme (Rothberg and Magleby, 1998). Uncoupled schemes have direct transition pathways between every open and closed state, and no transition pathways between open states or between closed states (Kienker, 1989). The log-likelihood value for the theoretical best fit for the simultaneous fitting of dwell-time distributions obtained at different Ca^{2+}_i was given by the sum of the log-likelihood values obtained by fitting data at each Ca^{2+} separately with the uncoupled scheme.

Using Simulation to Generate Predicted Single-Channel Data

To make comparisons between the observed distributions and those predicted by the kinetic models, simulated single-channel current records were generated with filtering equivalent to that used in the analysis of the experimental current records and with noise similar to that in the experimental current record. The simulated single-channel currents were then analyzed in the same way that the experimental currents were in order to obtain the predicted 2-D distributions, dependency plots, and numbers of exponential components observed in the predicted dwell-time distributions. The method used to simulate single-channel currents with filtering and noise is detailed in Magleby and Weiss (1990a). Visual comparison between observed and predicted distributions and dependency plots served to guide the analysis, indicate where models were inadequate, and give a sense for how well the models described the data. The critical assessment of the models was based on quantitative comparisons using maximum likelihood and Akaike rankings (Eqs. 3 and 4).

Online Supplemental Material

Figure S1 presents the equilibrium occupancy of the states in Scheme VII at low (5.5 μM) and high (1,024 μM) Ca^{2+}_i. At low Ca^{2+}_i, the channel spent most of its time (91.7%) in closed states C8–C11, considerably less time (7.5%) in open states O1–O6, and even less time (0.8%) in the intermediate closed states C12–C17. At high Ca^{2+}_i, the channel spent essentially all (99.4%) of its time in the fully liganded open and closed states, with most (96.6%) of the time spent in open states O1 and O4, considerably less time (2.8%) in closed states C7, C12, and C15. A very small amount of time (0.5%) was spent in open states O2 and O5, with negligible time (0.1%) spent in all of the remaining open and closed states. Thus, at high Ca^{2+}_i, Scheme VII gates as though there were one effective transition pathway between open and closed states (C15–O4), inconsistent with the observed significant dependencies at high Ca^{2+}_i. Available at http://www.jgp.org/cgi/content/full/114/1/93/DC1

Figure S2 presents the estimated rate constants for the three channels examined in detail for Schemes IV–VII, XII, and XIII. Available at http://www.jgp.org/cgi/content/full/114/1/93/DC1

results

The findings presented in this paper are based on a complete single-channel analysis of data obtained from three different BK channels, each studied at six different Ca^{2+}_i, from low to high (4–1,024 μM). In addition to these three channels, two additional channels were analyzed at three Ca^{2+}_i, including high Ca^{2+}_i, and an additional four channels were also examined, with findings consistent with the channels analyzed in more detail. All of the data, analysis, and figures presented in this paper are restricted to data collected during normal (mode) activity, which typically includes ~96% of the intervals (McManus and Magleby, 1988). All experiments were performed at +30 mV.

Saturation of P_o and the Mean Open and Closed Interval Durations at High Ca^{2+}_i

Currents flowing through a single BK channel in an inside-out patch of membrane excised from a cultured

rat skeletal muscle cell are shown in Fig. 1 A. These traces are representative of BK channel gating during normal activity over a range of Ca^{2+}_i, and illustrate a small fraction of the ~25 min of continuous recording from this channel. The current traces are excerpts of data obtained with 5.5, 12.3, 132, and 1,024 μM Ca^{2+}_i that gave mean open probabilities (P_o) during normal activity of 0.061, 0.50, 0.97, and 0.97, respectively. Thus, while the 2.2-fold increase in Ca^{2+}_i from 5.5 to 12.3 μM gave an 8.2-fold increase in P_o, the 7.8-fold increase in Ca^{2+}_i from 132 to 1,024 μM resulted in no increase in P_o, indicating that the channel had reached a maximum level of activation. The saturation in P_o at high Ca^{2+}_i is readily apparent in the current traces in Fig. 1.

The effect of Ca^{2+} on P_o for five different single BK channels during normal activity is illustrated in Fig. 2 A. For these channels, increasing Ca^{2+}_i in the 4–20 μM range increased P_o from ~0.02 to 0.85, while further increases in Ca^{2+}_i to either 132 or 1,024 μM led to a maximum P_o ranging from 0.93 to 0.98. Maximum P_os within this range have been observed previously (Barrett et al., 1982; Moczydlowski and Latorre, 1983; Rothberg et al., 1996; Cox et al., 1997a).

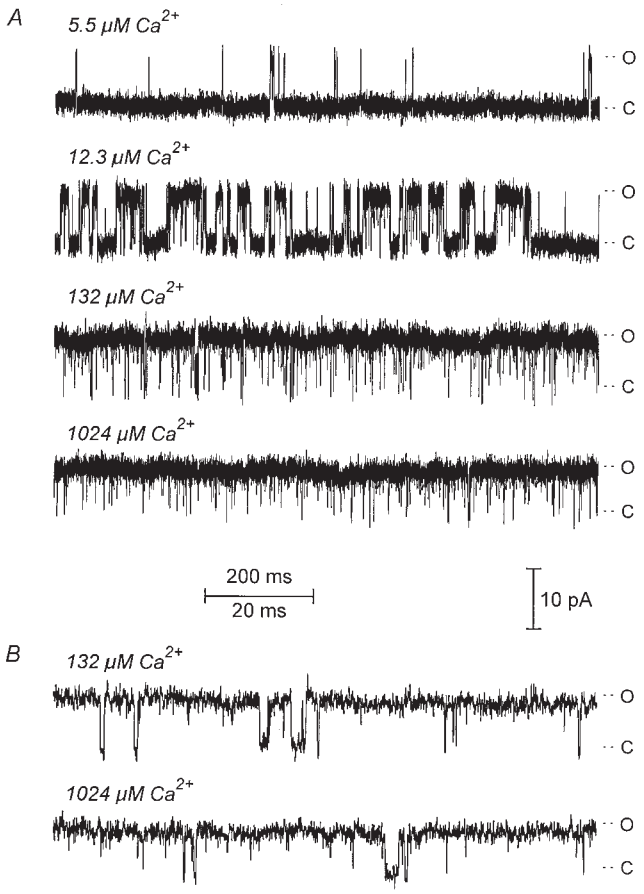

Figure 1. The gating of BK channels appears to kinetically saturate at high Ca^{2+}_i. (A) Representative currents recorded from a single BK channel at 5.5, 12.3, 132, and 1,024 μM Ca^{2+}_i and displayed at a time resolution of 1 s/trace. O and C indicate the open and closed current levels. (*B*) The currents recorded at high Ca^{2+}_i displayed at a time resolution of 100 ms/trace. All data in this and the following figures was collected at +30 mV.

Fitting P_o versus Ca^{2+}_i with the Hill equation for data from these five channels gave a $K_{0.5}$ (the Ca^{2+}_i for a P_o of 0.5) of 11.1 ± 0.7 μM, with a Hill coefficient of 3.5 ± 0.6, consistent with at least four Ca^{2+}-binding steps contributing to maximal channel activation. The mean of the maximal fitted P_o was 0.95 ± 0.03, and the fitted line indicated that a Ca^{2+} of ~40 μM was sufficient to drive the channel to within 1% of the maximum P_o. Hill coefficients ranging from 2–4 are a common feature of BK channels (see introduction), and higher slopes have been reported (Golowasch et al., 1986; Munoz et al., 1998), consistent with the channel binding at least four Ca^{2+} to become fully activated.

The P_o did not reach 1.0 during normal activity at high Ca^{2+}_i because of frequent sojourns to brief closed states that generated flickers, and also because of much less frequent sojourns to longer closed intervals with durations of typically 1–10 ms. Examples of the frequent flickers and of the less frequent longer closed intervals during normal activity at high Ca^{2+}_i (>100 μM) are presented in Fig. 1 B for data obtained at 132 and 1,024 μM Ca^{2+}_i. Analysis of the current records obtained at 132 and 1,024 μM Ca^{2+}_i indicated that only 2.1 ± 1.0% of the closed intervals had durations >1 ms, and even fewer, 0.026 ± 0.023%, had durations >10 ms. (The estimates obtained at both 132 and 1,024 μM Ca^{2+}_i from each of five channels were combined, as the percentages of longer closed intervals at the two different high Ca^{2+}_i were not significantly different.)

The increase in P_o with increasing Ca^{2+}_i was associated with increases in the mean open interval durations and decreases in the mean closed interval durations (Fig. 2, B and C), consistent with previous reports for BK channels from skeletal muscle (Barrett et al., 1982; Magleby and Pallotta, 1983; McManus and Magleby, 1991) and *mSlo* BK channels (Nimigean and Magleby, 1999).

The increase in mean open interval duration (Fig. 2 B, thick line; Hill coefficient of 1.02) was much less Ca^{2+} sensitive than the decrease in mean closed interval duration (Fig. 2 C, thick line; Hill coefficient of 3.48), suggesting that the major effect of Ca^{2+}_i is to decrease the durations of the closed intervals. The decreased filtering for channel B04 (Fig. 2 B, ◇) would contribute to the briefer observed open times for this channel, as more of the flickers would be captured.

Just as P_o saturated at high Ca^{2+}_i, the mean durations of the open and closed intervals also saturated in high Ca^{2+}_i at ~3.6 and ~0.15 ms, respectively (Fig. 2, B and C, thick line). Thus, any viable mechanism for the gating of the BK channel must account for a saturation in

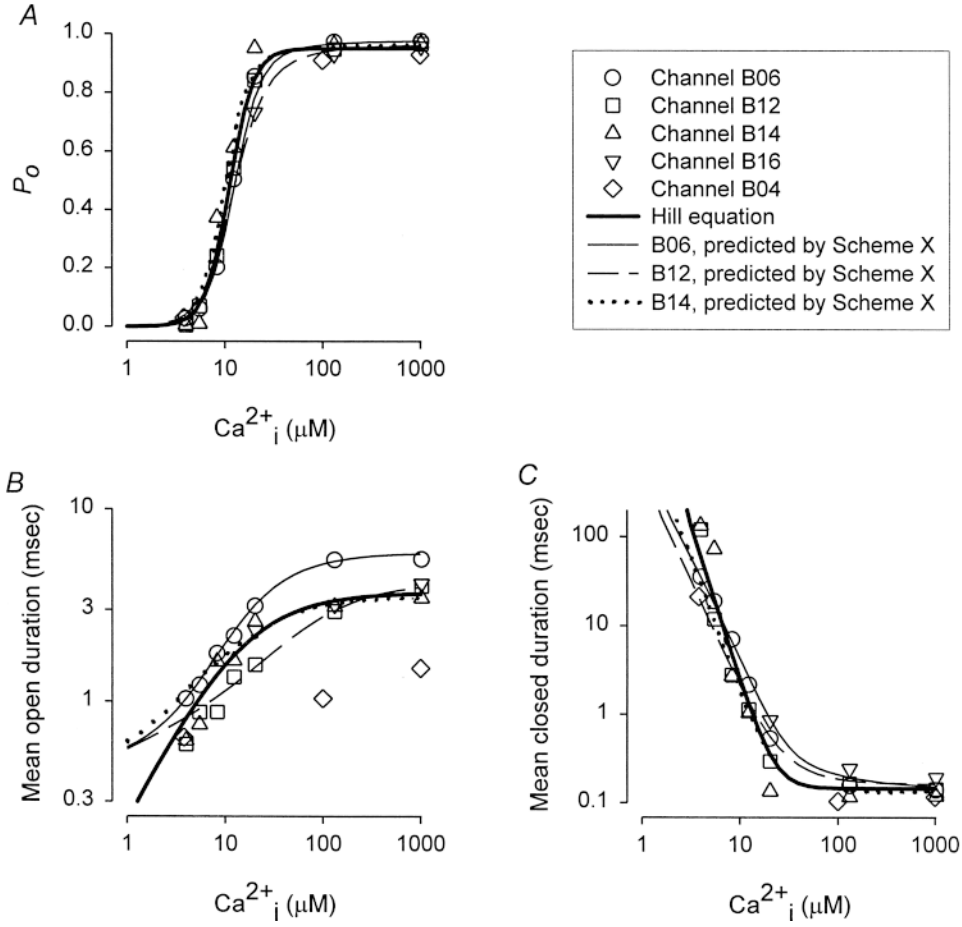

Figure 2. Increasing Ca^{2+}_i increases P_o and mean open interval duration and decreases mean closed interval duration. (A) Plot of P_o vs. Ca^{2+}_i for five single BK channels. The thick line represents a fit of the Hill equation to all the data points: $P_o = Max/[1 + (K_{0.5}/[Ca^{2+}_i])^n]$, where Max = 0.950 ms, $K_{0.5}$ = 11.1 μM, and n = 3.52. (B) Plot of mean open duration vs. Ca^{2+}_i for the same five channels. The thick line represents a fit of the Hill equation to all the data points, where Max = 3.68 ms, $K_{0.5}$ = 13.7 μM, and n = 1.02. (C) Plot of mean closed duration vs. Ca^{2+}_i for the same five channels. The thick line represents a fit of the equation $P_o = Min[1 + (K_{0.5}/[Ca^{2+}_i])^n]$, where Min = 0.145 ms, $K_{0.5}$ = 22.5 μM, and n = 3.48. (A–C) Predicted response of Scheme X for channel B06 (thin continuous line), channel B12 (dashed line), and channel B14 (dotted line, which is often superimposed on the thick line and not visible).

mean open times, mean closed times, and in P_o at high Ca^{2+}_i.

The Gating Kinetics Remain Unchanged at High Ca^{2+}_i

To further characterize the effect of high Ca^{2+}_i on gating, the open and closed interval durations during normal activity were measured and plotted as 1-D dwell-time distributions in Fig. 3. The thick lines in the open and closed distributions in Fig. 3 are the fits with mixtures (sums) of three open and five closed exponential components, respectively. Increasing Ca^{2+}_i from 5.5 to 132 μM shifted the open intervals to longer durations (note rightward shift of the major peak for the open times) and the closed intervals to briefer durations (note leftward shift and decreasing amplitude of the peak describing the longer closed times.). A further increase in Ca^{2+}_i from 132 to 1,024 μM had little additional affect on either the open or closed distributions, as seen in Fig. 3, D and H, where the fits to the distributions at 132 μM Ca^{2+}_i are plotted as thin lines on the fits to the distributions at 1,024 μM Ca^{2+}_i. The thin lines essentially superimpose the thick lines, indicating essentially unchanged gating kinetics at high Ca^{2+}_i. Fig. 3 H, inset, where the ordinate is plotted on a log scale to present the tails of the distributions at high gain, shows that the thin line also superimposes the thick line (within the range of the data) at the longer intervals where the frequency of occurrence of intervals is low. Results consistent with those in Fig. 3 were observed for four additional channels.

Table I presents the time constants and areas of the three open and five closed exponential components fitted to the 1-D distributions in Fig. 3. For increases in Ca^{2+}_i up to 132 μM, the time constant of the briefest open component remained relatively unchanged, the time constants of the two longer open components increased with increasing Ca^{2+}_i, and the area from the briefest open component shifted into the longer open components. In contrast, the time constants of the longer closed components became briefer and their areas shifted from the longer to the briefer closed components. Increasing the Ca^{2+}_i from 132 to 1,024 μM then had little additional effect on the open and closed components, when compared with the large effects observed for lower concentrations of Ca^{2+}_i.

Table II presents the mean ± SD of the time constants and areas of the exponential components for data obtained from five channels at two levels of high Ca^{2+}_i. For

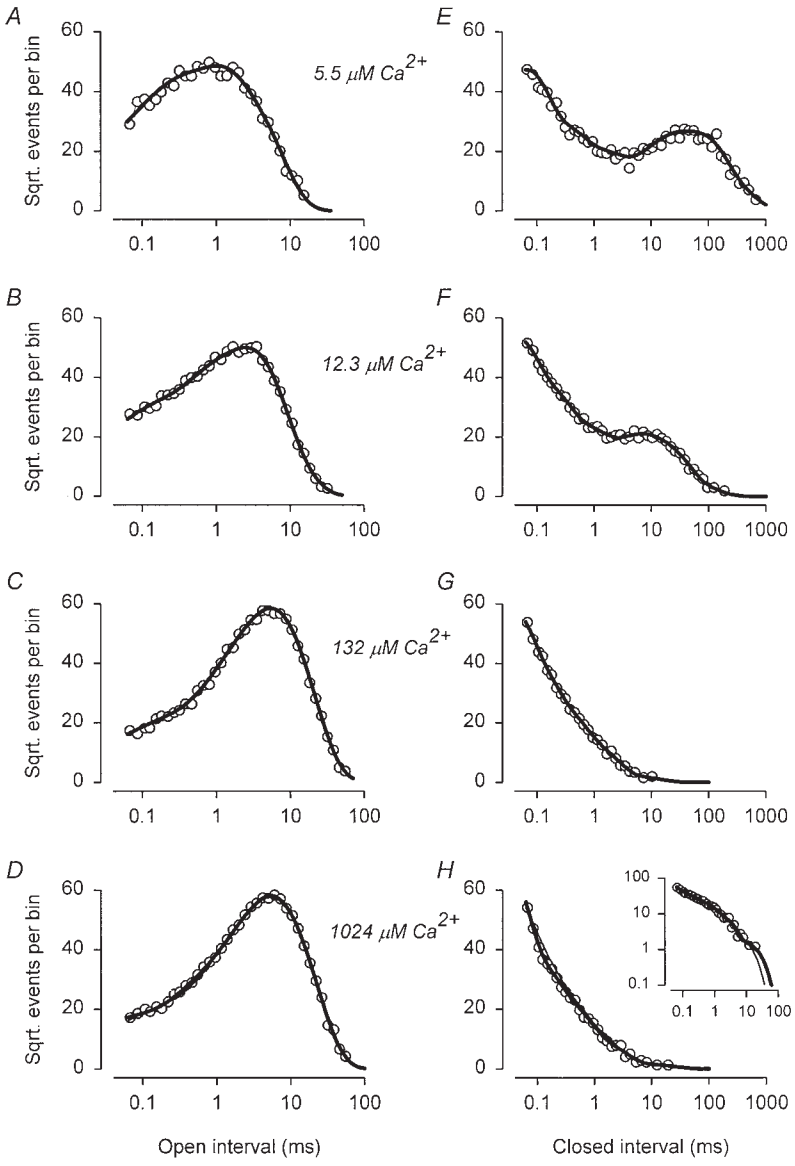

Figure 3. Open and closed 1-D dwell-time distributions obtained at 5.5, 12.3, 132, and 1,024 μM Ca^{2+}_i. The durations of open (A–D) and closed (E–H) intervals were log binned at a resolution of 25 bins/decade and plotted as the square-root of the number of intervals in each bin. The plotted open circles are the averages of two adjacent points to smooth the data for display. The thick lines plot the best fits of the distributions with mixtures of three open and five closed exponential components. The fits to the distributions at 132 μM Ca^{2+}_i (C and G) are replotted as thin lines on the distributions at 1,024 μM Ca^{2+}_i (D and H) to show that there is little difference between the distributions obtained at 132 and 1,024 μM Ca^{2+}_i. The closed distribution and fits shown in H are replotted on a logarithmic scale in the inset to allow high gain comparisons of the fits to the tails of the distributions. All distributions and fits were normalized to 100,000 intervals (integrated from time zero to infinity). The actual numbers of fitted intervals in each distribution were: 5.5 μM, 4,711 open and 3,848 closed; 12.3 μM, 13,520 open and 9,826 closed; 132 μM, 14,330 open and 7,725 closed; 1,024 μM, 18,128 open and 8,510 closed. Deadtime, 28.5 μs; channel B06.

four of the channels, the data were obtained at 132 and 1,024 μM Ca^{2+}_i, and for the fifth channel the data were obtained at 100 and 1,000 μM Ca^{2+}_i. The data from the fifth channel was pooled with the data from the other four since there was no apparent difference in the findings. Increasing the Ca^{2+}_i from 132 to 1,024 μM had no significant effect on either the time constants or areas of any of the open or closed components (Table II, $P > 0.05$; paired *t* test). The measured increase in the time constant of the slowest closed component in Table I for channel B06 would be consistent with stochastic variation, as there were <20 intervals contributing to this component at each of the two levels of high Ca^{2+}_i.

The apparent lack of effect of an eightfold increase in Ca^{2+}_i on the dwell-time distributions at high Ca^{2+}_i suggest that the rates for the transitions between states that dominate the gating at high Ca^{2+} are either Ca^{2+} independent or saturate at high Ca^{2+}. These possibilities will be considered later.

Lack of Discrete Ca Block with High Ca^{2+}_i

It is well established that Ba^{2+} produces discrete block of BK channels (Vergara and Latorre, 1983; Miller, 1987). If Ca^{2+} produces a similar block, then a potential difficulty with conducting experiments in high Ca^{2+}_i is the possibility of discrete (slow) channel block by Ca^{2+}. Closed intervals arising from discrete Ca^{2+} block could then be mistaken for closed intervals arising from sojourns to closed states during the gating. The observations in Figs. 1 and 3 at high Ca^{2+}_i are consistent with our previous findings of a lack of evidence for discrete Ca^{2+} block of native BK channels from rat skeletal muscle (Rothberg et al., 1996). Increasing

TABLE I

Time Constants and Areas of Fitted Exponential Components at the Indicated Ca^{2+}_i

	5.5 μM		12.3 μM		132 μM		1024 μM	
Component	τ	Area	τ	Area	τ	Area	τ	Area
	ms		*ms*		*ms*		*ms*	
Open distributions								
1	0.17	0.225	0.13	0.143	0.12	0.047	0.13	0.047
2	0.79	0.406	0.94	0.226	4.26	0.409	3.25	0.262
3	2.21	0.370	3.01	0.631	6.72	0.544	6.69	0.691
Closed distributions								
1	0.06	0.516	0.04	0.528	0.03	0.585	0.02	0.753
2	0.30	0.162	0.15	0.249	0.08	0.266	0.09	0.162
3	1.52	0.073	0.71	0.098	0.24	0.113	0.30	0.072
4	27.3	0.131	7.10	0.088	0.80	0.036	1.13	0.013
5	102	0.119	21.2	0.037	4.02	0.001	7.08	0.0004

Channel B06.

TABLE II

Time Constants and Areas of Fitted Exponential Components at High Ca^{2+}_i

	132 μM		1024 μM	
Component	τ	Area	τ	Area
	ms		*ms*	
Open distributions				
1	0.09 ± 0.04	0.062 ± 0.020	0.09 ± 0.03	0.057 ± 0.018
2	1.85 ± 1.65	0.208 ± 0.149	1.64 ± 1.38	0.163 ± 0.116
3	3.71 ± 2.01	0.772 ± 0.160	4.31 ± 1.88	0.813 ± 0.131
Closed distributions				
1	0.03 ± 0.008	0.601 ± 0.019	0.02 ± 0.003	0.659 ± 0.058
2	0.11 ± 0.06	0.276 ± 0.040	0.09 ± 0.03	0.235 ± 0.060
3	0.35 ± 0.23	0.093 ± 0.038	0.042 ± 0.40	0.087 ± 0.032
4	0.87 ± 0.27	0.028 ± 0.015	0.87 ± 0.19	0.022 ± 0.008
5	4.2 ± 1.5	0.003 ± 0.003	4.5 ± 1.7	0.002 ± 0.002

Values are means ± SD for five channels, except for open component 2, which is based on data from four channels.

Ca^{2+}_i eightfold from 132 to 1,024 μM had little effect on the closed dwell-time distributions (Fig. 3, C, D, G, and H). If appreciable closed intervals arose from discrete Ca^{2+} block, then increasing Ca^{2+}_i eightfold might have been expected to have a noticeable effect on the distributions, which was not observed.

As a more critical test for discrete block, we tabulated the frequency of occurrence of closed intervals >1 and >10 ms at the two different Ca^{2+}_i. For the five examined BK channels, the frequency of closed intervals with durations >1 ms was 7.4 ± 3.6 s^{-1} for 132 μM Ca^{2+}_i and 5.6 ± 2.5 s^{-1} for 1,024 μM Ca^{2+}_i, values that were not significantly different ($P = 0.098$, paired t test). The frequency of closed intervals with durations >10 ms was 0.12 ± 0.11 s^{-1} with 132 μM Ca^{2+}_i and 0.076 ± 0.086 s^{-1} with 1,024 μM Ca^{2+}_i, values that were also not significantly different ($P = 0.44$, paired t test).

Thus, the lack of effect of Ca^{2+} on the closed dwell-time distributions from brief to long times, and also on all closed intervals >1 and >10 ms, suggests that discrete Ca^{2+} block did not contribute to the closed intervals. As expected, increasing Ca^{2+}_i to 1,024 μM did decrease the conductance of the channel by ~10%, presumably due to a screening (fast blocking) effect (Ferguson, 1991). Cox et al. (1997a) studying *mSlo* BK channels also found that high Ca^{2+}_i (1,000 μM) reduced single-channel conductance through a fast block, but did not induce discrete block. Since high Ca^{2+}_i does not introduce closed intervals arising from discrete block, it is possible to estimate the numbers of kinetic states that contribute to the gating at high Ca^{2+}_i.

At Least Three to Four Open and Four to Five Closed States Are Entered during Gating in High Ca^{2+}_i

Assuming that the gating is consistent with a discrete-state Markov model (McManus and Magleby, 1989; Petracchi et al., 1991), the number of significant exponential components required to describe the dwell-time distributions gives an estimate of the minimum number of states entered during the gating (Colquhoun and Hawkes, 1981, 1995a). Estimates of the numbers of significant exponential components were made from fitting both 1-D and 2-D dwell-time distributions (see methods). (Examples of 1-D distributions were presented in Fig. 3 and examples of 2-D distributions will be presented in a later section.) These estimates were then plotted against Ca^{2+}_i in Fig. 4.

In general, the 1-D and 2-D methods gave similar estimates of the numbers of exponential components, but there were some differences. 2-D fitting can have an increased ability to detect components over 1-D fitting when the same numbers of intervals are analyzed (Rothberg et al., 1997). However, with 2-D fitting, when very brief intervals pair with longer intervals, both intervals in the pair are excluded from the fitting to avoid potential artifacts arising from fitting intervals with durations <1.5–2 dead times (see methods). The combination of the greater ability to detect components together with the fitting of fewer intervals for 2-D fitting, when compared with 1-D fitting, would contribute to the minor differences in the numbers of significant components estimated by the 1- and 2-D fitting methods.

At the lower concentrations of Ca^{2+}_i, the distributions were typically described by three to four open and four to seven closed components for fitting with either 1- or 2-D distributions (Fig. 4), consistent with previous observations (McManus and Magleby, 1988; Wu et al., 1995; Rothberg and Magleby, 1998). At the high concentrations of 132 and 1,024 μM Ca^{2+}_i, the open distributions were still typically described by three to four open components, and the closed distributions were

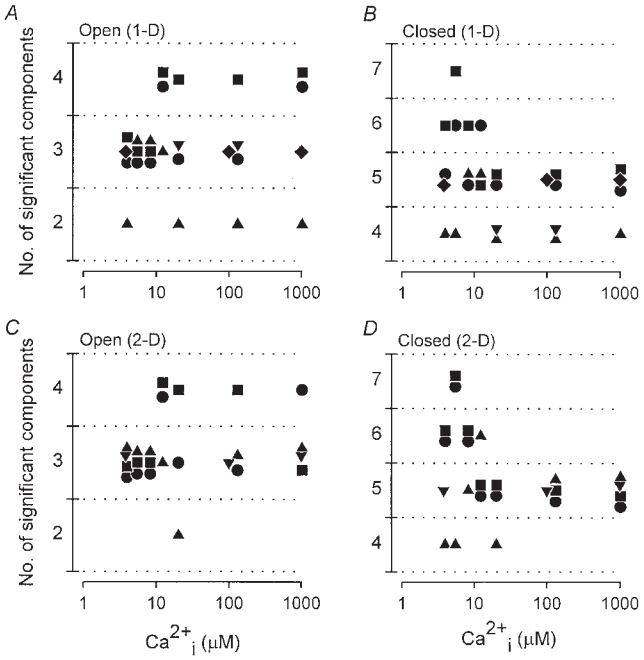

Figure 4. Numbers of significant exponential components determined from maximum likelihood fitting of dwell-time distributions are plotted as a function of Ca^{2+}_i. Points have been offset vertically to prevent overlap. (A) Numbers of significant open components estimated from fitting 1-D open dwell-time distributions with mixtures of 1-D exponential components. (B) Numbers of significant closed components estimated from fitting 1-D closed dwell-time distributions. (C and D) Numbers of significant open and closed components estimated from fitting 2-D (open–closed) dwell-time distributions with mixtures of 2-D exponential components. With 2-D fitting, the numbers of open and closed components are determined within a single fit. The symbols for five different channels are: B06 (●), B12 (■), B14 (▲), B16 (▼), and B04 (◆).

typically described by four to five closed components. Thus, at kinetically saturating levels of Ca^{2+}_i, the gating typically involved transitions among at least three to four open and four to five closed kinetic states.

Theoretical Models for the Gating of Tetrameric Ligand-gated Channels

Functional BK channels can be formed by four alpha subunits (Shen et al., 1994), and the BK channels in skeletal muscle, as studied here, are unlikely to be associated with the auxiliary beta subunit that increases the Ca^{2+} sensitivity of the channel (Tseng-Crank et al., 1996; Chang et al., 1997; Nimigean and Magleby, 1999). If one or more Ca^{2+} ions bind to each alpha subunit to fully activate the channel (Schreiber and Salkoff, 1997), then this would give a basis for the high Hill coefficients of 2–4 that are typically observed for activation (see introduction).

Although relatively simple in concept, with four subunits and at least one Ca^{2+}-binding site per subunit, theoretical models for the gating of a ligand-activated homotetramer, such as the BK channel, can be highly complex, with 35–55 potential states (Eigen, 1969; Cox et al., 1997b). The 55-state model (Cox et al., 1997b) is given by Scheme I, where each subunit can assume either of two conformations, indicated by squares or circles, and each subunit in either conformation can either be free of Ca^{2+} (open symbols) or bound with a Ca^{2+} (shaded symbols). Many of the states are isoforms, in which subunits with diagonal and adjacent conformational changes and Ca^{2+} bindings have potentially different functional properties.

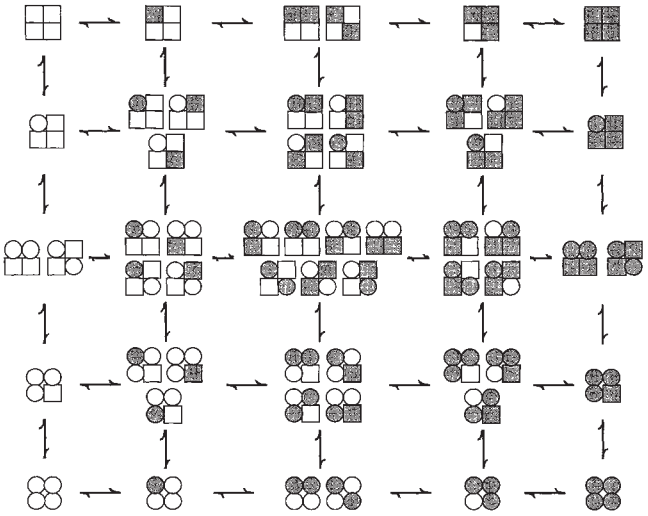

(scheme i)

For the gating of the channel, the states in the top row of Scheme I are assumed to represent closed states of the channel, and the states in the bottom row are assumed to represent open states. The conductance of the states in the middle three rows is less clear, but may be open, closed, or partially conducting (Cox et al., 1997a). Scheme I reduces to the 35-state model of Eigen (1968) if it is assumed that diagonal and adjacent subunits in the same conformation have identical properties. Because of the complexity of the 55- and 35-state schemes, Scheme I is often reduced further to the 25-state model described by Scheme II (Fersht, 1985).

If it is further assumed that each collection of isoforms has the same properties, and that conformational changes are concerted so that all four subunits undergo conformational changes simultaneously or that the lifetimes of the middle three rows of states in Schemes I and II are very brief, then Schemes I and II reduce to the 10-state Monod-Wyman-Changeux model for allosteric proteins (Monod et al., 1965) described by Scheme III.

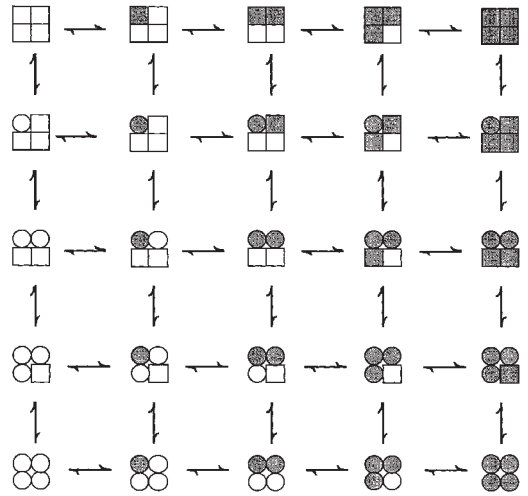

(scheme ii)

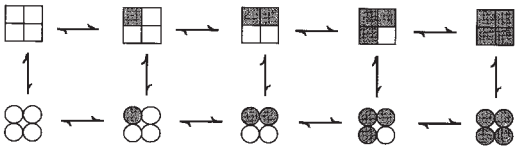

(scheme iii)

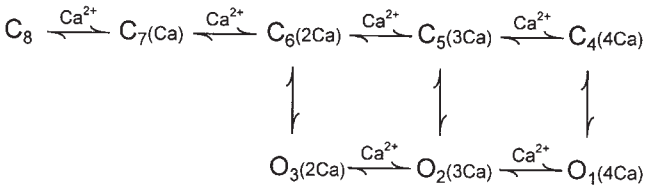

(scheme iv)

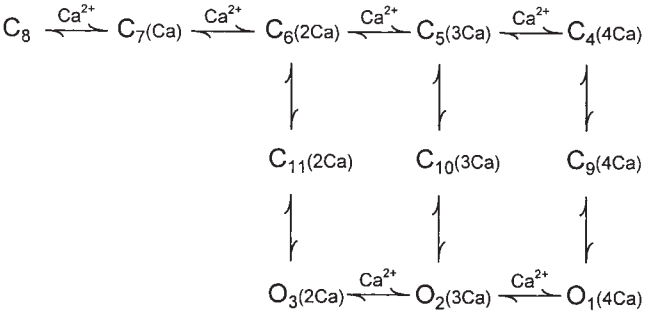

(scheme v)

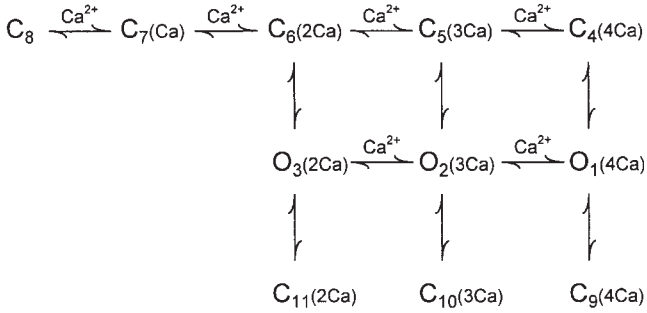

(scheme vi)

Simple Models Fail to Predict the Single-Channel Kinetics at High Ca^{2+}_i

It has been shown previously for low to intermediate levels of Ca^{2+}_i that the Ca^{2+} dependence of the single-channel kinetics of BK channels in rat skeletal muscle can be approximated by the gating mechanisms described by Schemes IV–VI (McManus and Magleby, 1991; Rothberg and Magleby, 1998). Thus, we first examined whether these schemes might also account for the single-channel kinetics through high Ca^{2+}_i.

Scheme IV is drawn from the MWC model. Scheme VI is an expansion of Scheme IV because it includes closed states beyond the activation pathway. Scheme V can be viewed as a condensed version of Schemes I and II if it is assumed that the intermediate states in Schemes I and II are too brief to be detected or that only a subset can be detected. It is the additional brief closed states C9, C10, and C11 that generate most of the flickers (brief closings) in Schemes V and VI, whereas flickers for Scheme IV are generated mainly by sojourns between states O2 and C5. Flickers are highly characteristic of single-channel currents and can be seen in Fig. 1.

Before examining whether Schemes IV–VI could account for the gating from low through high Ca^{2+}_i, we first examined whether they could describe the 1-D dwell-time distributions from low to intermediate levels of Ca^{2+}_i, as reported previously (McManus and Magleby, 1991; Rothberg and Magleby, 1998). Rate constants for each scheme were estimated by the simultaneous fitting of 2-D dwell-time distributions obtained at three different Ca^{2+}_i of 5.5, 8.3, and 12.3 μM (see methods). The most likely rate constants were then used to simulate single-channel data with noise and filtering equivalent to that of the experimental data. The simulated current records were then analyzed in the same manner as the experimental data to determine the predicted 1-D dwell-time distributions. As expected, the predicted distributions gave excellent descriptions of the observed 1-D dwell-time distributions from low to intermediate Ca^{2+}_i for the three channels examined in detail. For example, for the data in Fig. 3, A, B, E, and F, at 5.5 and 12.3 μM Ca^{2+}_i, the predicted distributions typically overlapped or were within a line width of the thick lines describing the dwell-time distributions in these figures (not shown).

We next examined whether Schemes IV–VI could predict the distributions from low to high Ca^{2+}_i. Rate

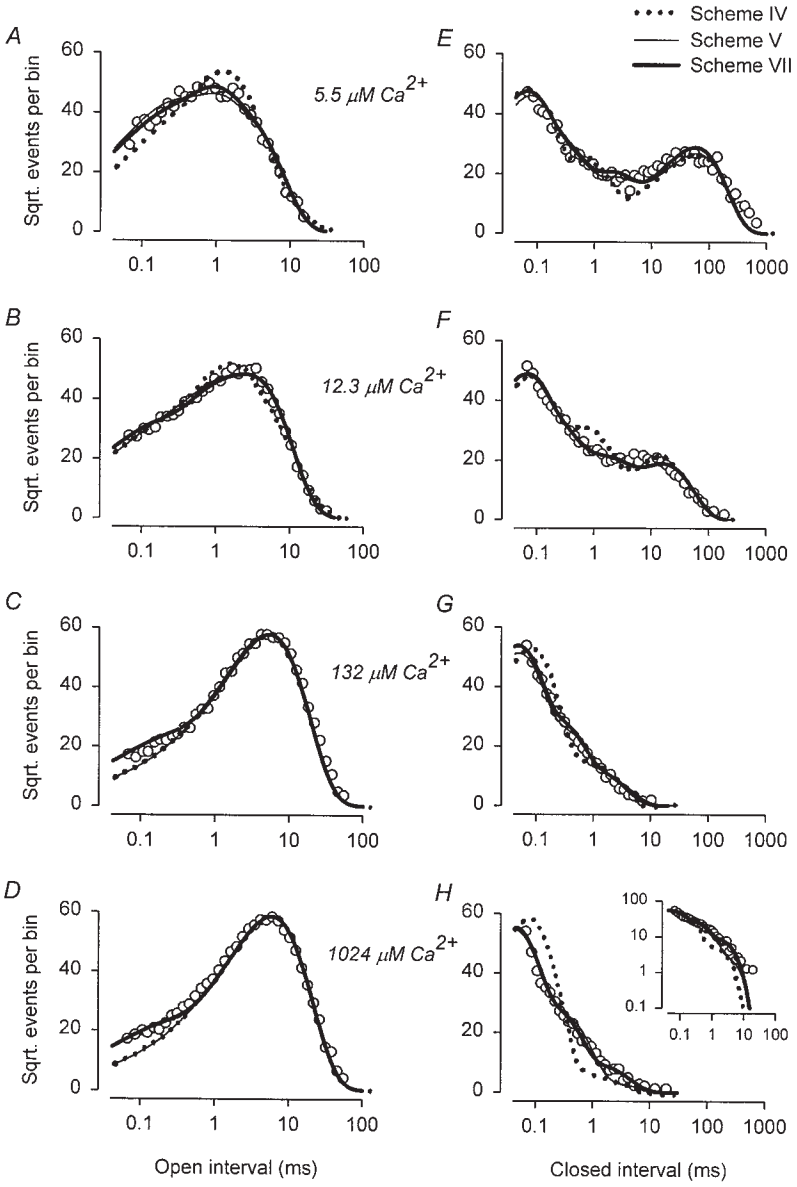

Figure 5. Schemes IV and V cannot account for the 1-D dwell-time distributions from low to high Ca^{2+}_i, while Schemes VII and X can. (A–H) The predicted distributions for Schemes IV (dotted lines), V (thin lines), and VII (thick lines) are plotted with the experimental data (○) from Fig. 3. Scheme X predicted distributions that essentially superimposed the thick line for Scheme VII. The rate constants used in the predictions were obtained by simultaneous maximum likelihood fitting of 2-D distributions obtained at six different Ca^{2+}_i ranging from 5.5 to 1,024 μM. The fitted rate constants were then used with the schemes to predict the distributions. The distribution and fits in H are replotted on a logarithmic scale as an inset. Deadtime, 28.5 μs; channel B06.

constants for each scheme were estimated by the simultaneous fitting of 2-D dwell-time distributions obtained at six different Ca^{2+}_i of 5.5, 8.3, 12.3, 20.3, 132, and 1,024 μM. These rate constants were then used to predict the observed distributions over the full range of Ca^{2+}_i. As shown in Fig. 5, Scheme IV could not simultaneously describe the dwell-time distributions from low to high Ca^{2+}_i. Scheme V gave a better description than Scheme IV, but still could not describe the distributions. The predictions of Scheme VI were very slightly better than those of Scheme V, and are not shown. Table III shows the schemes rankings: Scheme VI > Scheme V > Scheme IV (Akaike rankings, Eq. 4).

The inability of these schemes to account for the single-channel kinetics from low to high Ca^{2+}_i indicates that the models described by Schemes IV–VI are too simple. Such a finding is, perhaps, not surprising since Scheme IV with eight states and Schemes V and VI with 11 states include only a small subset of the minimal 55 potential states for the gating of a ligand-activated homotetrameric channel based on theoretical considerations (Scheme I). Nevertheless, it is possible that the channel does not gate as described by the theoretical 55-state model or, if it does, that only a fraction of the potential 55 states actually contribute to the gating. Consequently, we examined the differences between the observed and predicted responses for these schemes to determine how the minimal schemes might be expanded to be more consistent with the gating of the channel.

For high Ca^{2+}_i, Schemes IV–VI predicted fewer brief openings than were observed in the single-channel

TABLE III

Normalized Likelihood Ratios (NLR_{10000}) and Rankings (R) of Schemes IV–X

Scheme	Channel 1 (B06)		Channel 2 (B12)		Channel 3 (B14)	
	NLR_{1000}	R	NLR_{1000}	R	NLR_{1000}	R
IV	3.15 ± 10^{-33}	6	8.66 ± 10^{-30}	6	3.63 ± 10^{-41}	6
V	8.54 ± 10^{-10}	5	4.74 ± 10^{-13}	5	5.35 ± 10^{-15}	5
VI	1.04 ± 10^{-9}	4	5.37 ± 10^{-13}	4	6.25 ± 10^{-15}	4
V-sat	3.15 ± 10^{-5}	3	3.66 ± 10^{-6}	3	1.01 ± 10^{-6}	3
VII	8.79 ± 10^{-5}	2	1.22 ± 10^{-5}	2	1.24 ± 10^{-6}	1
X	3.25 ± 10^{-4}	1	1.24 ± 10^{-5}	1	1.25 ± 10^{-6}	2

V-sat is Scheme V with saturation in the binding of Ca^{2+} for the data collected at 132 and 1,024 μM Ca^{2+}_i (see text).

data (Fig. 5). Brief openings in Scheme V typically arose from sojourns such as -C11-O3-C11-, and in Scheme VI from sojourns such as -C11-O3-C11- or -C6-O3-C6-, as O3 was the open state with the briefest lifetime in both schemes. For these schemes, the channel would be unlikely to reach O3 or the associated closed states at high Ca^{2+}_i, as the high Ca^{2+}_i would drive the gating towards the fully liganded states. Thus, to generate more brief open intervals at high Ca^{2+}_i, there needs to be a means for the gating to reach directly one or more brief open states from the fully liganded closed states. In addition, the underprediction of the long closed intervals at high Ca^{2+}_i suggests that the channel may also gate among additional closed states at high Ca^{2+}_i not included in Schemes IV–VI. Further evidence that the channel gates among additional states at high Ca^{2+}_i arises from the observation in Fig. 4 that the channels typically entered at least three to four open and four to five closed states at high Ca^{2+}_i, while analysis of the dwell-time distributions predicted by Schemes IV–VI at high Ca^{2+}_i indicated that the distributions were described by only one open and two to three closed components.

Scheme VII Can Describe the Open and Closed 1-D Dwell-Time Distributions from Low to High Ca^{2+}_i

We next examined how Scheme V might be expanded to provide the required access to more open and closed states at high Ca^{2+}_i. Scheme V is contained within the general Schemes I and II if it is assumed that the three rows of intermediate states in the general schemes are closed states that can be collapsed into one row of brief lifetime intermediate closed states. However, since it is possible that the last two rows of states in Schemes I and II are open states and that the remaining intermediate closed states do not collapse into one row of closed states, we investigated whether simplified schemes drawn from Scheme II, with an assumption of three rows of closed states and two rows of open states, could account for the data.

Scheme VII presents a gating mechanism of this type, where open states O4-O5-O6 (with brief lifetimes) and closed states C12-C13-C14 are the additional rows of open and closed states when compared with Scheme V. With high Ca^{2+}_i, the channel could now make sojourns from closed states to brief open states, such as -C15-O4-C15-, giving brief open intervals, and also make sojourns from closed states to longer open (and compound open) states, such as -C15-O4-O1-O4-C15-, giving longer open intervals. The extra row of closed states should also allow the generation of longer closed intervals at high Ca^{2+}_i by allowing more sojourns among closed states between openings.

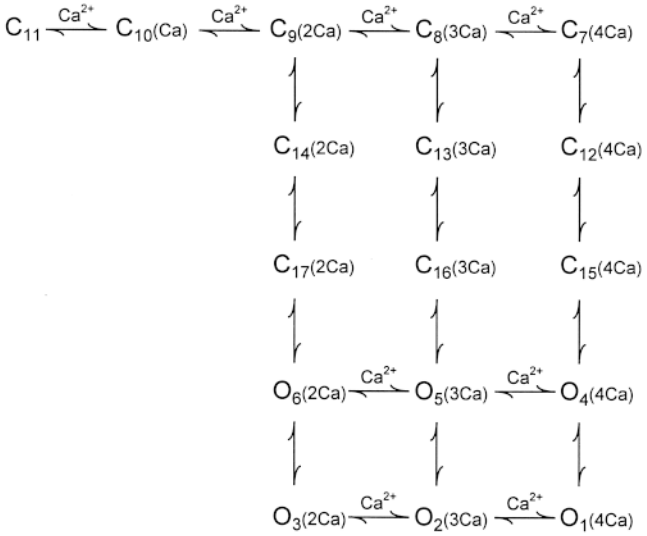

(scheme vii)

The most likely rate constants for Scheme VII were determined from the simultaneous fitting of 2-D dwell-time distributions at six different Ca^{2+}_i (5.5, 8.3, 12.3, 20.3, 132, and 1,024 μM). The thick lines in Fig. 5 show that the additional states allowed Scheme VII to describe the 1-D open and closed dwell-time distributions from low to high Ca^{2+}_i. In this scheme, the mean lifetimes at 5.5 μM Ca^{2+}_i of states O4, O5, and O6, of 0.11, 0.09, and 0.03 ms, tend to be brief compared with the lifetimes of the final row of open states O1, O2, and O3 of 0.50, 0.18, and 0.06 ms. The improved ability of Scheme VII to describe the single-channel gating when compared with Schemes IV–VI (compare thick line to dotted and thin lines in Fig. 5) is also reflected in the greatly improved likelihood ratios in Table III.

We also examined whether a scheme like Scheme VII, but with one less row of intermediate closed states, could account for the data. For the three channels examined, the likelihood estimates were two to four orders of magnitude less than for Scheme VII, and the reduced scheme ranked below Scheme VII for all three channels (not shown).

Scheme VII accounts for the 1-D open and closed dwell-time distributions from low to very high Ca^{2+}_i (Fig. 5). Such a description would be sufficient to predict P_o as a function of Ca^{2+}_i over a wide range of activity, but the 1-D distributions do not take into account the correlation information between adjacent intervals, which can give insight into the connections (transition pathways) among the various states (Magleby and Song, 1992; Rothberg and Magleby, 1998). To examine the correlation information, we determined whether Scheme VII could account for the kinetic structure of the single-channel data. The kinetic structure is described by 2-D dwell-time distributions and dependency plots. The 2-D distributions indicate the frequency of occurrence of pairs of adjacent open and closed intervals (Fredkin et al., 1985; Magleby and Weiss, 1990b), and the dependency plots convey information about the correlations of adjacent interval durations (Magleby and Song, 1992).

The kinetic structure for the same channel featured in the previous figures (channel B06) is shown in Fig. 6 at four different Ca^{2+}_i. The 2-D dwell-time distributions (Fig. 6, left) are plotted on log–log coordinates with the logs of the durations of adjacent open and closed intervals locating the position of the bin on the x and y axis, respectively. The z axis plots the square root of the numbers of intervals in each bin. These 2-D dwell-time distributions thus extend the Sigworth and Sine (1987) transform used in the previous figures to two dimensions. From the 2-D dwell-time distributions it can be seen that pairs of long open intervals adjacent to brief closed intervals (flickers) occur most frequently of all the interval pairs, and this is the case from low to high Ca^{2+}_i (Fig. 6, left, position 4). It is these interval pairs that give rise to the characteristic longer openings separated by flickers in the experimental data (Fig. 1). At the lowest Ca^{2+}_i of 5.5 μM, there were also large numbers of longer open intervals adjacent to longer closed intervals (Fig. 6, left, position 6) and brief open intervals adjacent to longer closed intervals (left, position 3). As the Ca^{2+}_i was raised, the longer closed intervals shifted to briefer durations. The peak at position 6 with 5.5 μM Ca^{2+}_i shifted towards position 5 at 12.3 μM Ca^{2+}_i, and position 4 at higher Ca^{2+}_i.

The dependency plots in Fig. 6 (right) present the fractional excess or deficit of interval pairs of specified durations over that expected if the intervals paired at random. Dependencies of +0.5 or −0.5 would indicate a 50% excess or 50% deficit of interval pairs over the number expected if open and closed intervals paired independently. The thick lines indicate a dependency of zero. Because the dependency plots present magnified representations of excesses and deficits in the numbers of observed interval pairs relative to the numbers expected for independent pairing, they must be interpreted with some caution, as the estimates of dependency can be unreliable where the numbers of observed interval pairs per bin in the 2-D dwell-time distributions are small. Consequently, references to dependency will only be made when the referenced dependencies are known to be significantly different from zero. Such dependencies will be referred to by numbers on the dependency plots. Examples of which areas of the dependency plots are significantly different from zero are presented in Rothberg and Magleby (1998) for low to intermediate levels of Ca^{2+}_i and will be presented in a later section for data obtained at high Ca^{2+}_i.

The dependency plots in Fig. 6 (right) indicate that over the wide range of examined Ca^{2+}_i there was a deficit of brief open intervals adjacent to brief closed intervals (position 1), an excess of brief open intervals adjacent to both intermediate and long closed intervals (positions 2 and 3), and a deficit of long open intervals adjacent to long closed intervals (position 6; not clearly visible in the presented orientation, but visible when the plots were rotated). At the lower Ca^{2+}_i of 5.5 and 12.3 μM, there was also an excess of longer open intervals adjacent to brief closed intervals (position 4). These specific excesses and deficits of interval pairs give rise to the characteristic saddle shape of the dependency plots for BK channels (Rothberg and Magleby, 1998), and were consistently seen for all the examined channels.

While the kinetic structure at intermediate levels of Ca^{2+}_i for six different BK channels has been presented previously (Rothberg and Magleby, 1998), it was important to determine whether the kinetic structure at high Ca^{2+}, as shown in Fig. 6, was consistently observed. (It will be shown in a later section that the presence or absence of significant dependencies at high Ca^{2+}_i is a key factor in distinguishing gating mechanism.) Fig. 7 presents such plots for data obtained at 132 and 1,024 μM Ca^{2+}_i for two additional channels. Although there were some obvious differences in the magnitudes of the dependencies, the general shape of the kinetic structure in these plots was the same as for the channel shown in Fig. 6, G and H, in that there were obvious deficits of brief open intervals adjacent to brief closed intervals (Fig. 7, right, position 1) and obvious excesses of brief open intervals adjacent to intermediate duration closed intervals (right, position 2).

Dependency significance plots were made for the data obtained at high Ca^{2+}_i to estimate which dependencies were significantly different from zero. A paired *t* test was used to compare the number of interval pairs in each bin of the observed 2-D dwell-time distribution with the number expected if adjacent open and closed intervals paired independently, by using a moving 3 ×

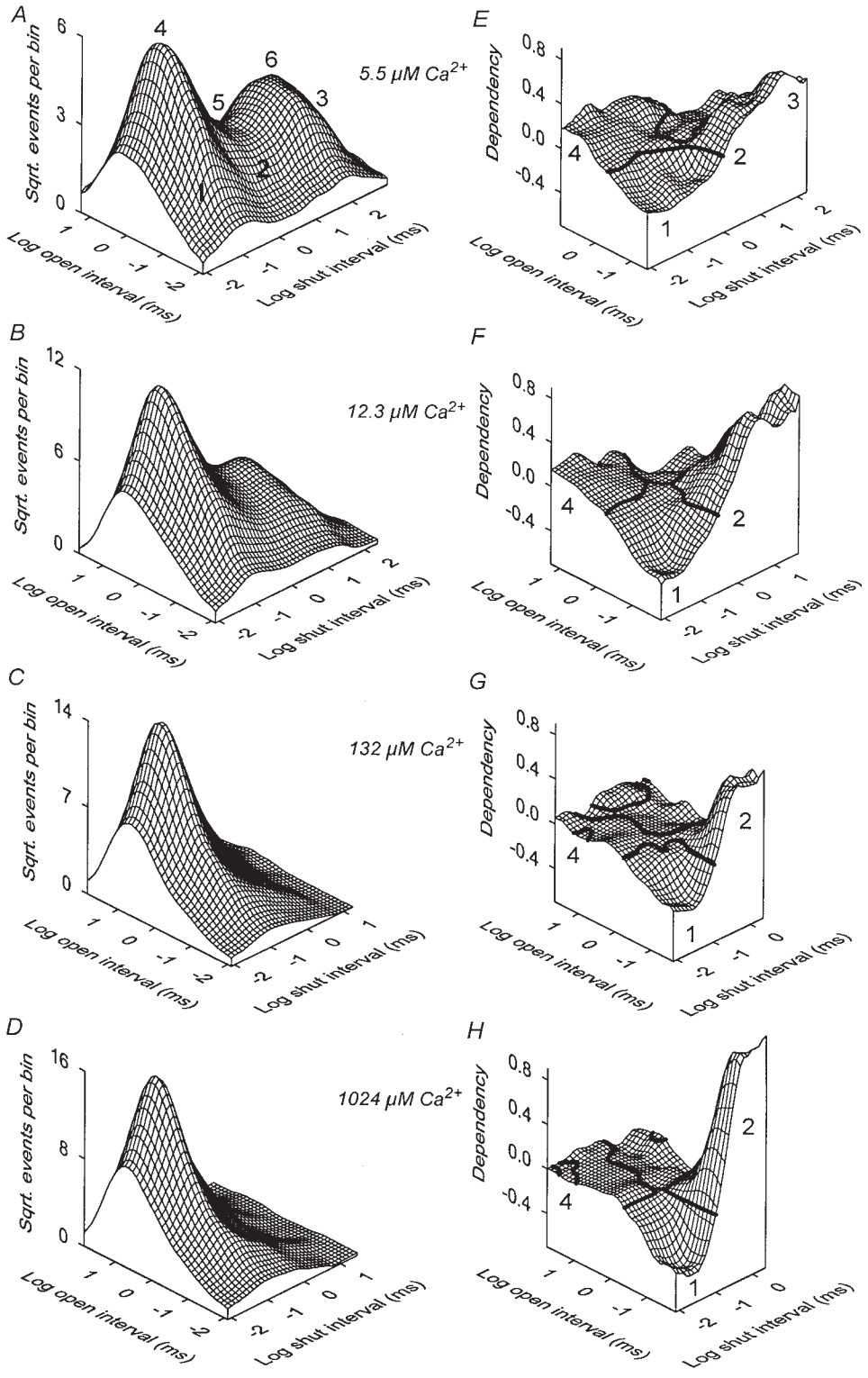

Figure 6. Kinetic structure of a BK channel at 5.5, 12.3, 132, and 1,024 μM Ca^{2+}_i. (A–D) 2-D dwell-time distributions. Adjacent open and closed intervals were binned as pairs, with the logs of the open and closed interval durations locating the bins on the x and y axes, respectively. The z axis plots the square root of the number of intervals in each bin. (E–H) Dependency plots, which present the fractional excess and deficit of interval pairs in the observed 2-D dwell-time distributions in A–D when compared with the 2-D dwell-time distributions calculated assuming independent pairing of open and closed intervals (Eq. 1). The thick lines indicate a dependency of zero. Channel B06.

3 bin array as detailed in Rothberg and Magleby (1998). Results are shown in Fig. 8 for channel B12. The plots in Fig. 8, A and C, present the dependency significance for the front and back views, respectively, of the dependency plot in Fig. 7 E obtained at 132 μM Ca^{2+}_i, and the plots in Fig. 8, B and D, present the dependency significance for the front and back views of the dependency plot in Fig. 7 F obtained at 1,024 μM Ca^{2+}_i. The dependency significance plots present the logarithm of the estimated *P* value, which is multiplied

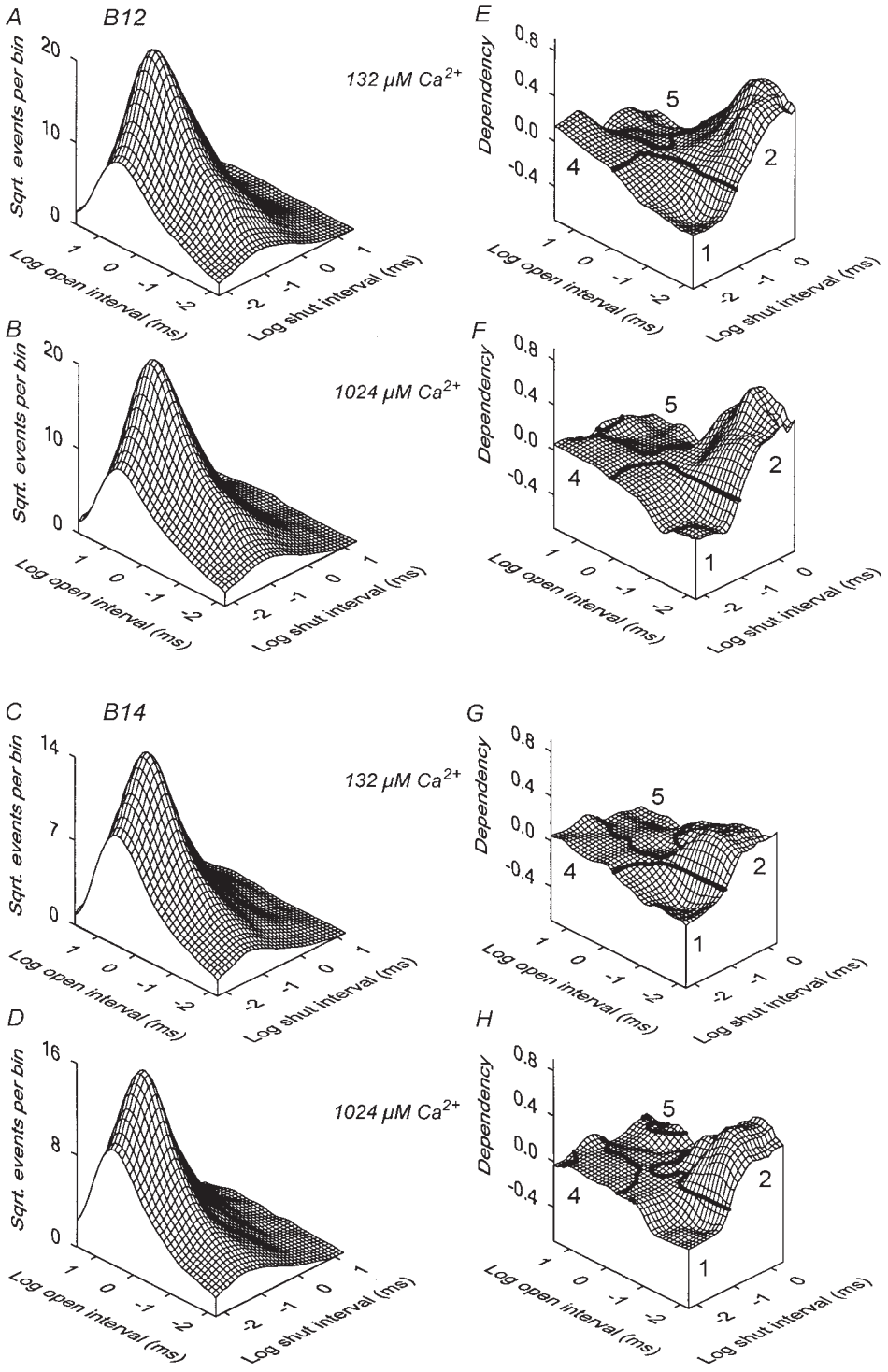

Figure 7. Adjacent open- and closed-interval durations are dependent at high Ca^{2+}_i. The kinetic structure is presented at two different levels of high Ca^{2+}_i for channels B12 and B14. The deficit of intervals at position 1 and the excess of intervals at position 2 are consistently seen. The approximately eightfold increase in Ca^{2+}_i from 132 to 1,024 μM has little effect on either the 2-D dwell-time distributions or the dependency plots.

by the sign of the dependency to indicate whether the paired intervals are in excess or deficit. The thick lines on the plots at −1.3 and 1.3 indicate a significance level of $P = 0.05$. Absolute values of dependency significance > 1.3, 2, 3, and 4 would indicate $P < 0.05$, 0.01, 0.001, and 0.0001, respectively.

From Fig. 8 it can be seen that the dependencies at the numbered positions 1, 2, 4, and 5 were significantly different from zero at both 132 and 1,024 μM Ca^{2+}_i. Importantly, there was a significant excess of long open intervals adjacent to brief closed intervals (position 4), even though the fractional excess of these interval pairs was small in the dependency plots (Fig. 7, E and F). The reason for this apparent discrepancy is that most of

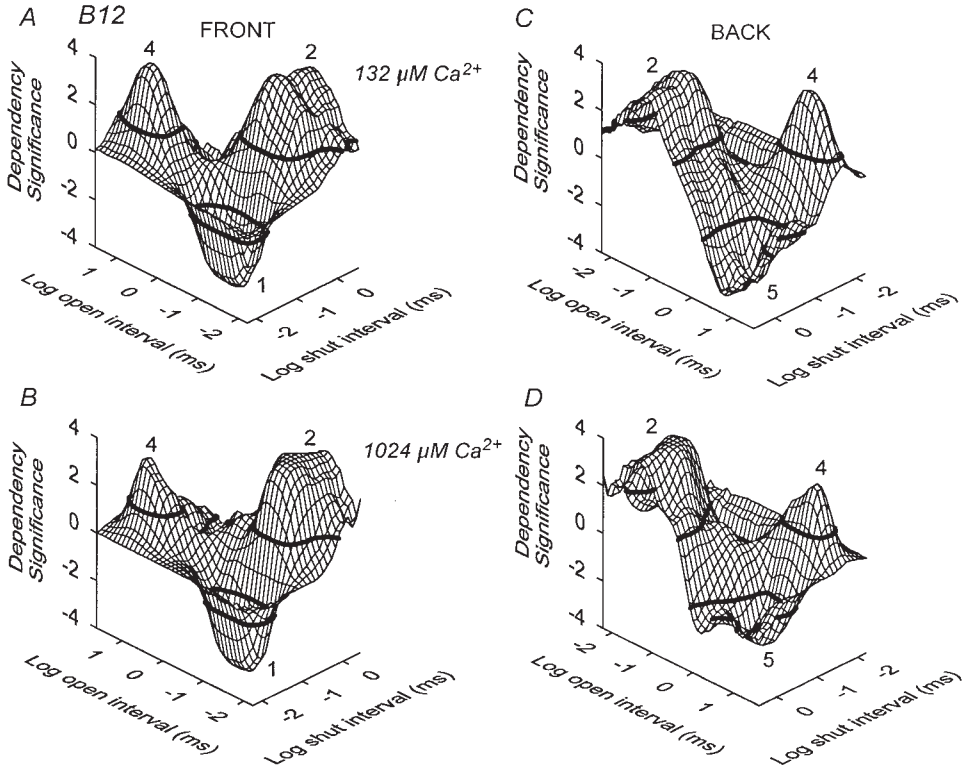

Figure 8. The dependencies at positions 1, 2, 4, and 5 in the dependency plots obtained at high Ca^{2+}_i are significantly different from zero. (A–B) The significance of the dependencies in the dependency plots in Fig. 7, E and F, are plotted as dependency significance, which indicates the log of the *P* value times the sign of the dependency at each location. Absolute values of dependency significance greater than the thick lines at +1.3 and −1.3 indicate that the dependency values are significant ($P < 0.05$). Absolute values of dependency significance >2 and >3 would indicate $P < 0.01$ and 0.001, respectively. (C–D) Reverse-angle views of the plots in A and B, respectively. Channel B12.

the interval pairs fall at position 4 in high Ca^{2+}_i, as can be seen from the 2-D dwell-time distributions (Fig. 7, A–D), so that even an appreciable excess of interval pairs at position 4 would still appear small when plotted as dependency, which plots the fractional excess of intervals (Eq. 1). In six of six dependency significance plots that were examined at high Ca^{2+}_i, the dependencies at positions 1, 2, and 5 were significant, and the dependency at position 4 was significant in five of six plots. The one plot where significance was not observed at position 4 had fewer numbers of analyzed intervals.

The observations that the numbers of detected kinetic states remained relatively unchanged from low to high Ca^{2+}_i (Fig. 4) and that the general shapes of the dependency plots also remained relatively unchanged from low to high Ca^{2+}_i (Figs. 6 and 7) raise the possibility that the basic gating mechanism remains relatively unchanged from low to high Ca^{2+}_i.

Scheme VII Describes the Kinetic Structure at Low but not High Ca^{2+}_i

To determine whether Scheme VII could account for the kinetic structure, the most likely rate constants for Scheme VII, determined from the simultaneous fitting of 2-D dwell-time distributions at six different Ca^{2+}_i (5.5, 8.3, 12.3, 20.3, 132, and 1,024 μM), were used to simulate single-channel data for Scheme VII with noise and filtering equivalent to that of the experimental data. The simulated current records were then analyzed in the same manner as the experimental data to determine the predicted kinetic structure shown in Fig. 9.

Scheme VII captured the basic features of the kinetic structure at 5.5 and 12.3 μM Ca^{2+}_i (compare the predicted 2-D dwell-time distributions and dependency plots in Fig. 9, A, B, E and F, to the observed plots in Fig. 6, A, B, E, and F). Scheme VII also captured the basic features of the 2-D dwell-time distributions at the high Ca^{2+}_i of 132 and 1,024 μM (compare Fig. 9, C and D with Fig. 6, C and D). However, Scheme VII predicted that little or no dependence would be observed at high Ca^{2+}_i (Fig. 9, G and H), in contrast to the significant dependencies observed in the experimental data (Fig. 6, G and H, and Figs. 7 and 8). Thus, Scheme VII predicted that open and closed intervals would pair randomly at high Ca^{2+}_i, in contrast to the dependent pairing observed in the data. These observations indicate that Scheme VII is too simple to capture the features of the gating at high Ca^{2+}_i.

The Gating Is Effectively Restricted to the Fully Liganded States of Scheme VII at High Ca^{2+}_i

To explore why Scheme VII did not predict the dependency at high Ca^{2+}_i, we calculated the equilibrium occupancies of the various open and closed states for this scheme. At low to intermediate Ca^{2+}_i (5.5–12.3 μM), the channel readily entered all the states in Scheme VII, with occupancy biased towards the closed states

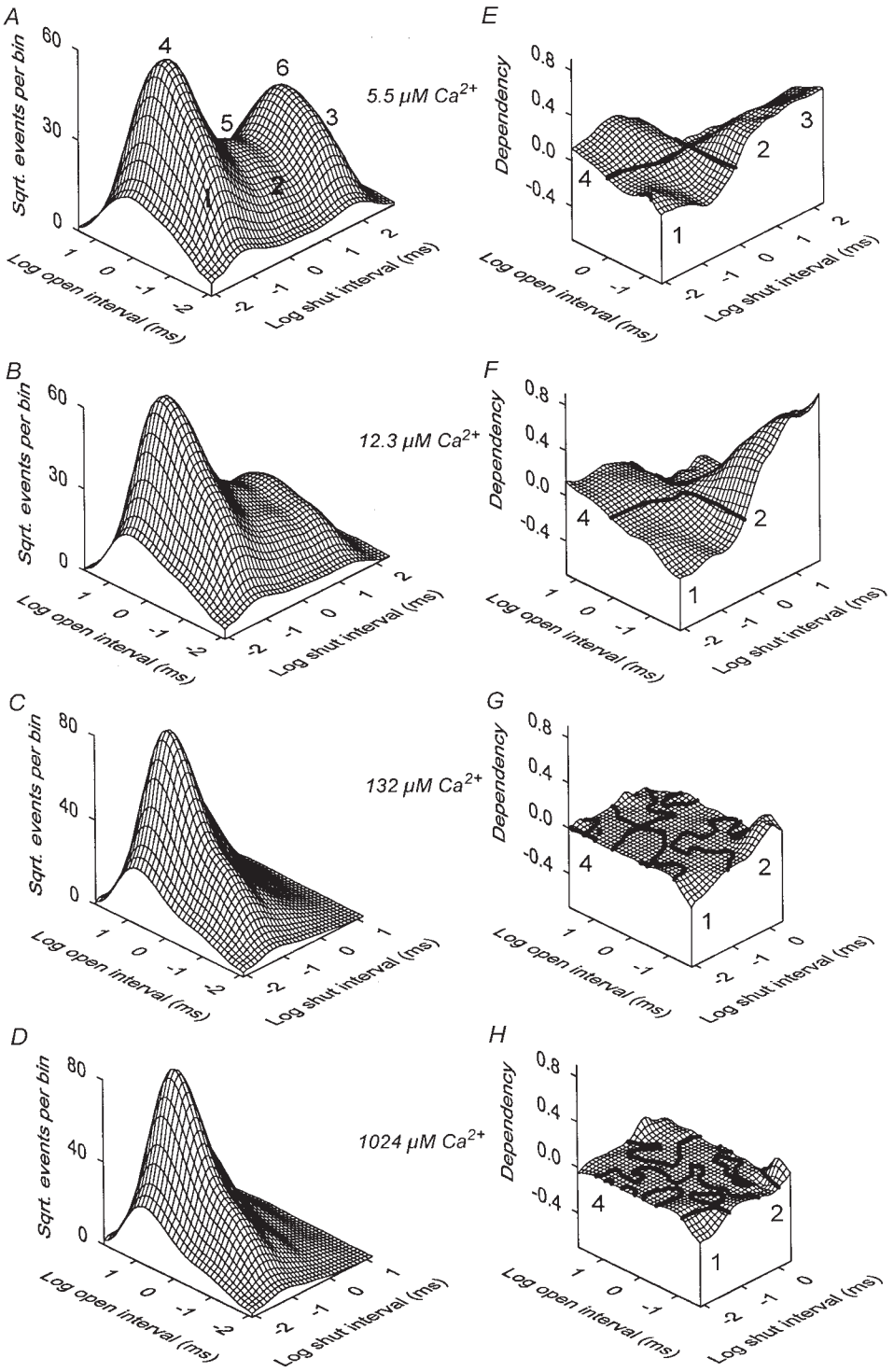

Figure 9. Scheme VII describes the basic features of the kinetic structure from low to intermediate Ca^{2+}_i, but cannot describe the kinetic structure at high Ca^{2+}_i. (A–H) Kinetic structure predicted by Scheme VII from low to high Ca^{2+}_i. Scheme VII predicted little dependence at high Ca^{2+}_i. (Compare with the experimental data in Fig. 6.) The rate constants used in the predictions were obtained by simultaneous maximum likelihood fitting of 2-D distributions obtained at six different Ca^{2+}_i ranging from 5.5 to 1,024 μM. Scheme VII with the same rate constants could predict the 1-D dwell-time distributions in Fig. 5 (thick line). Channel B06.

C8–C11 at the low Ca^{2+}_i. At high Ca^{2+}_i (132 and 1,025 μM), the channel spent 99.6% of its time in the fully liganded states, with 96.6% in open states 1 and 4 and 2.8% in closed states 7, 12, and 15. (The calculated equilibrium occupancies for Scheme VII can be found in online supplemental Figure S1 [http://www.jgp.org/cgi/full/114/1/93/DC1].)

The reason that Scheme VII predicted a lack of dependence between adjacent open and closed intervals at high Ca^{2+}_i is now readily apparent. Because the channel spent 99.4% of its time in the fully liganded column of states at high Ca^{2+}_i, the channel would essentially gate as Scheme VIII. Scheme VIII has a single effective transition pathway between the open and

closed states, given by C15-O4. A single effective transition pathway gives a single gateway state, which would lead to independent pairing of open and closed intervals and lack of significant dependencies (McManus et al., 1985; Colquhoun and Hawkes, 1987; Song and Magleby, 1994).

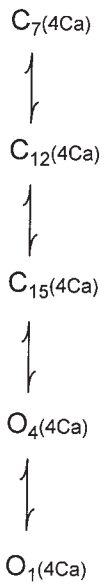

(scheme viii)

If Scheme VII does effectively gate in the fully liganded column of states at high Ca^{2+}_i, as indicated by Scheme VIII, then a maximum of two open and three closed components would be detected in the dwell-time distributions predicted by Scheme VII at high Ca^{2+}_i. This was found to be the case. Fitting exponentials to dwell-time distributions simulated with Scheme VII at high Ca^{2+}_i gave two open and three closed components, compared with the typically three to four open and four to five closed states detected in the experimental data. Scheme VII also predicted a lack of dependence and too few components at high Ca^{2+}_i for the two other channels analyzed in detail.

Schemes I, II, and VII Can Be Rejected

The above findings indicate that Scheme VII can thus be rejected as a model for gating, as it cannot describe the dependencies at high Ca^{2+}_i. By analogy, Schemes I and II and all schemes based on subsets of states drawn from these schemes, such as Schemes II–VI, can also be rejected as such schemes would also not describe the dependencies at high Ca^{2+}_i, provided that the forward rate constants for binding of Ca^{2+} are sufficiently rapid at high Ca^{2+} to effectively keep the gating in the fully liganded column of states.

The Kinetic Structure at High Ca^{2+}_i Suggests a Two-Tiered Gating Mechanism

The above results suggest that models for gating at high Ca^{2+}_i must: (a) allow effective transitions among at least three to four open and four to five closed states at high Ca^{2+}_i to generate the required numbers of exponential components in the dwell-time distributions (Fig. 4), (b) have two or more independent transition pathways between open and closed states (two or more gateway states) at high Ca^{2+}_i to generate a dependent relationship between the durations of adjacent intervals (Figs. 6–8), and (c) gate among the three to four open and four to five closed states at high Ca^{2+}_i in a manner that is essentially independent of Ca^{2+}_i for $Ca^{2+}_i > 100$ μM to account for the observed lack of effect of Ca^{2+} on the gating at high Ca^{2+}_i (Figs. 1–3 and Tables I and II).

Since Schemes I and II are theoretical schemes based on a ligand-activated homotetramer, it might be useful if these schemes could be modified to account for gating at high Ca^{2+}_i. As pointed out by Cox et al. (1997b), it is not necessarily clear which of the states in Scheme I are open and which are closed. Perhaps all 55 (Scheme I) or 25 (Scheme II) states are closed, each with the potential of opening through a concerted conformational change of the subunits. Concerted conformational changes leading to opening have been suggested previously for the gating of *Shaker* channels (Bezanilla et al., 1994; Zagotta et al., 1994; Zheng and Sigworth, 1998). If each closed state can open for BK channels, then Schemes I and II would become two-tiered 110- and 50-state models, respectively, with the upper tiers composed entirely of closed states and the lower tiers of an equal number of open states. Preliminary data using macroscopic ionic and gating currents from *mSlo* are consistent with such models (Horrigan and Aldrich, 1998). The extension of Scheme II to a two-tiered model is given by Scheme IX, where in the graphic representation all 25 closed states in the upper tier are visible and only the first two rows of the 25 open states in the lower tier are visible

Scheme X Can Approximate the Kinetic Structure From Low to High Ca^{2+}_i

A difficulty with Scheme IX, as was also the case for Schemes I and II, is that Scheme IX has so many rate constants that it would be difficult if not impossible to determine unique rate constants for this scheme, even by the simultaneous fitting of 2-D dwell-time distributions over a range of Ca^{2+}_i (see methods). Consequently, we examined whether a reduced version of Scheme IX might be sufficient to approximate the kinetic structure. The number of rows of closed states in the upper tier was reduced from five to three, and the number of rows of open states in the lower tier was re-

duced from five to two to obtain the reduced Scheme X. Some of the open and closed states with zero and one bound Ca^{2+} were also omitted in Scheme X to reduce further the number of rate constants because, over the range of Ca^{2+}_i examined in this paper, it might be expected that these states would contribute little to the gating (Cui et al., 1997; Rothberg and Magleby, 1998).

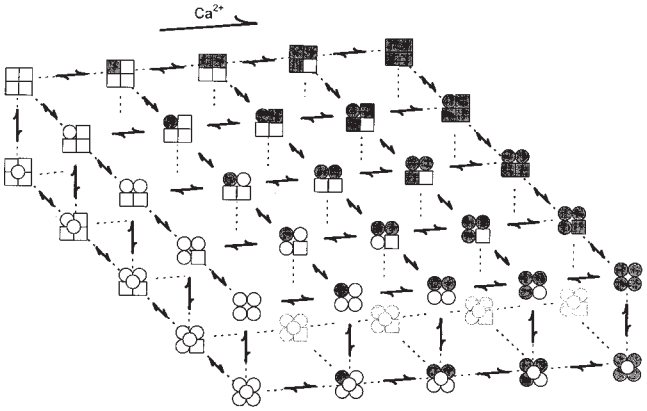

(scheme ix)

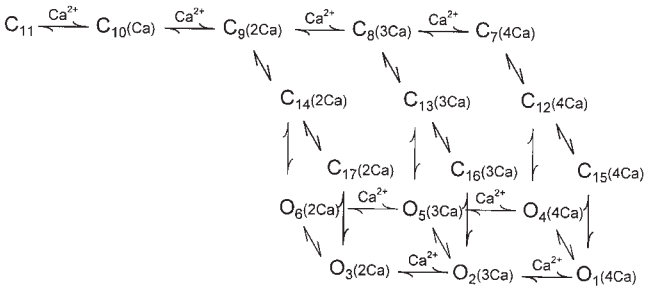

(scheme x)

Scheme X is like Scheme VII, except that Scheme X has a total of six independent transition pathways between the open and closed states, compared with three in Scheme VII. Two of the independent transition pathways connect fully liganded open and closed states, which would then allow at least two functional gateway states for gating with high Ca^{2+}_i. Two or more gateway states would be needed to generate the dependencies observed in high Ca^{2+}_i.

Scheme X was tested by determining the most likely rate constants from the simultaneous fitting of 2-D dwell-time distributions obtained at six different Ca^{2+}_i ranging from 5.5 to 1,024 μM. The most likely rate constants were then used with Scheme X to obtain the predicted kinetic structure in Fig. 10. The predicted kinetic structure (compare to the observed in Fig. 6) shows that Scheme X captured the major features from low to high Ca^{2+}_i, including the general shapes of the dependency plots at high Ca^{2+}_i. Scheme X predicted the excess of brief open intervals adjacent to the longer closed intervals (position 2) and the deficits of brief open intervals adjacent to brief closed intervals (position 1) that were not predicted by Scheme VII at high Ca^{2+}_i (compare Fig. 10, G and H, with Figs. 9 and 6, G and H). For intervals with durations less than ~0.05 ms, Scheme X predicted too great of a deficit at position 1. This could reflect an inadequacy of the model or it could reflect the fact that dwell times <0.05 ms were not fitted, so that the predictions of the model were not constrained below this time.

As would be expected from the reasonable descriptions of the kinetic structure, Scheme X also described the Ca^{2+} dependence of the 1-D dwell-time distributions. The distributions predicted by Scheme X essentially superimposed the thick lines in Fig. 5. Scheme X also described the Ca^{2+} dependence of P_o and of the mean open and closed interval durations (Fig. 2, thin, dotted, and dashed lines).

Assessing the Various Gating Mechanisms

Scheme X could also describe the kinetic structure obtained from the two other channels examined over a wide range of Ca^{2+}_i. The rankings of the various kinetic schemes for the three channels together with the NLR_{1000} are presented in Table III. The NLR_{1000}, which gives a measure of how well the schemes describe the data (see below and methods), indicated that Scheme X was more likely than the other examined schemes for all three channels (larger values of NLR_{1000} are more likely).

While the NLR_{1000} can indicate which schemes are most likely, it does not apply any penalties for additional free parameters. Consequently, the schemes were ranked by the Akaike criteria, which applies a penalty for additional free parameters (Eq. 4). The general rankings were: Scheme X > Scheme VII > Schemes IV–VI (Table III). The Akaike test ranks schemes, but does not give the significance of the rankings. The likelihood ratio test can be used to estimate the significance of rankings for nested models (Horn and Lange, 1983; see examples in McManus and Magleby, 1988). Schemes VII and X ranked significantly above Schemes IV–VI and V-sat ($P < 0.001$) for all three channels. Interestingly, Scheme X ranked above Scheme VII for only two of three channels, and this ranking was significant for only one channel (B06, $P < 0.001$) in spite of the fact that Scheme X gave better likelihoods than Scheme VII for all three channels.

The apparent discrepancy between visual observations and the significance of some of the rankings may reflect the necessarily conservative nature of statistical tests. Alternatively, the discrepancy may reflect that Scheme X is still too simple, so that obvious improvements in some aspects of the gating, such as in the dependency plots, are countered by minimal improvements or even small detrimental changes in other as-

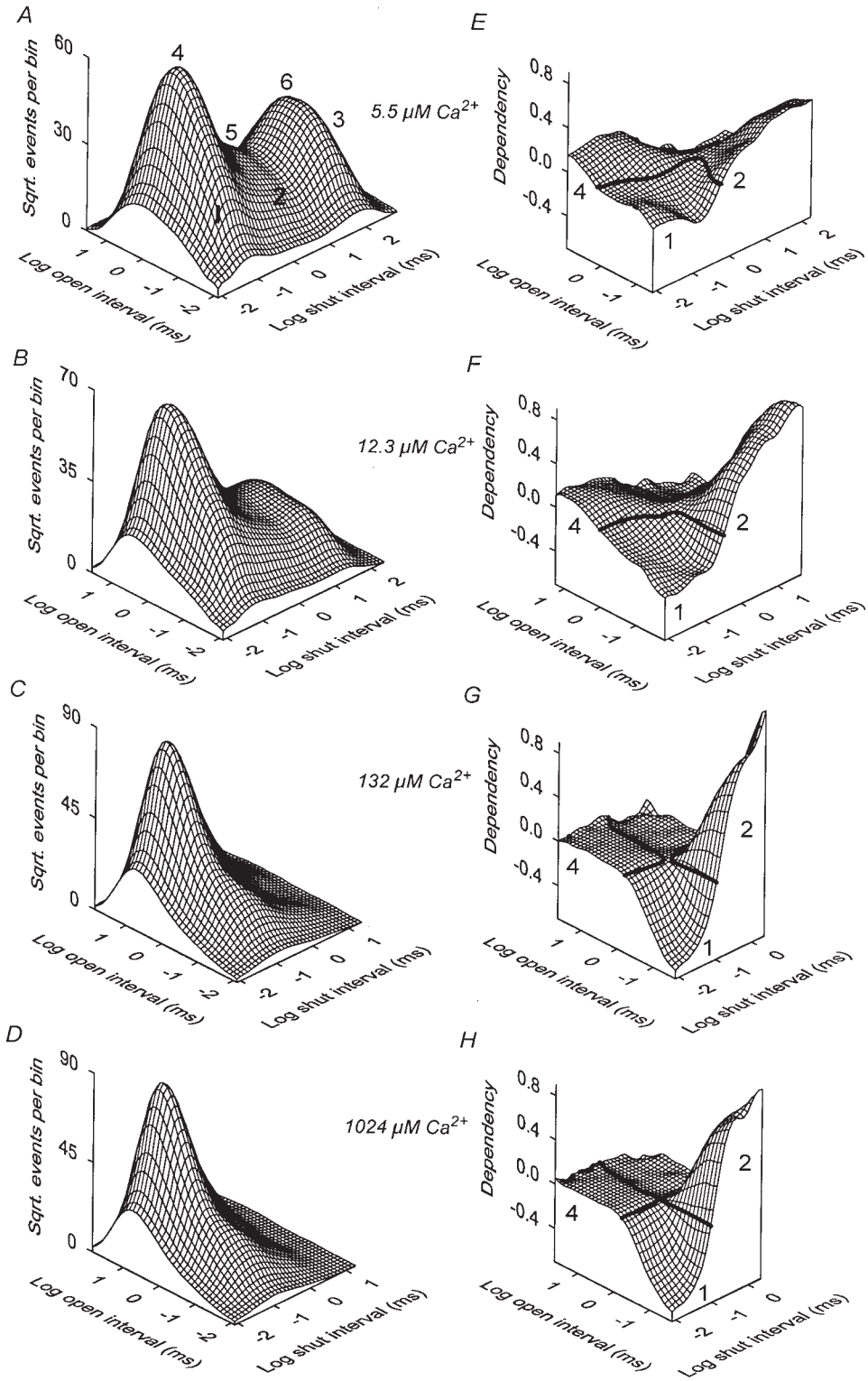

Figure 10. The two-tiered Scheme X describes the basic features of the kinetic structure from low to high Ca^{2+}_i. (A–H) Kinetic structure predicted by Scheme X. (Compare with the experimental data in Fig. 6.) The rate constants used in the predictions were obtained by simultaneous maximum likelihood fitting of 2-D distributions obtained at six different Ca^{2+}_i ranging from 5.5 to 1,024 μM. Channel B06.

pects of the gating. Thus, Scheme X may have to be expanded into Scheme IX to obtain sufficiently improved descriptions of the data to outweigh the heavy penalty imposed by the ranking tests. Consistent with this possibility, Scheme X predicts only two open and three closed exponential components at high Ca^{2+}_i. It will be shown in a later section that the gating of the fully liganded channel is described better by models that more closely approximate Scheme IX.

The NLR_{1000} values in Table III give a numerical measure of how well the various schemes describe the experimental data. A NLR of 1.0 indicates that a kinetic scheme

describes the 2-D dwell-time distributions as well as the theoretical best description for a discrete state Markov model (see methods). The thick lines in Fig. 3 show the theoretical best description of the 1-D distributions. For channel B06, the values of NLR_{1000} (normalized to 1,000 interval pairs) ranged from 3.15×10^{-33} for Scheme IV to 3.25×10^{-4} for Scheme X. These values give likelihood ratios per interval pair of 0.93 $[(3.15 \times 10^{-33})^{0.001}]$ for Scheme IV and 0.99 $[(3.25 \times 10^{-4})^{0.001}]$ for Scheme X. Such values suggest an average likelihood difference per interval pair between the predicted and theoretical best fits of 7% for Scheme IV and only 1% for Scheme X. The 7% difference per interval pair is readily seen (Fig. 5, dotted line), while the small 1% difference is still visually apparent as less than perfect descriptions of the data (Fig. 5, thick line, and compare Fig. 10 to Fig. 6).

Scheme X Predicts too Few Components at High $Ca^{2+}{}_i$

In spite of its relative success, Scheme X is still too simple. Analysis of simulated data indicated that Scheme X predicted only two significant open and four significant closed components at high $Ca^{2+}{}_i$, compared with the three to four open and five closed components in the experimental data. This underprediction is not surprising, since for Scheme X the high $Ca^{2+}{}_i$ would effectively drive the gating towards the two open and three closed fully liganded states.

Models for the Gating of the Fully Liganded Channel

Since Scheme X predicts too few components at high $Ca^{2+}{}_i$, we explored what types of gating mechanisms might be consistent with the gating at high $Ca^{2+}{}_i$. In theory, Scheme IX could be examined directly, but the data would be insufficient to constrain the large numbers of rate constants for the 50-state model. Consequently, we explored the reduced models given by Schemes XI–XIII, which are all composed of fully liganded states.

Scheme XI is drawn from the 10-state model describing the fully liganded states in Scheme IX (the rightmost column of states) with two open states excluded because they had no significant effect on the likelihood estimates. Scheme XII expands Scheme XI so that transitions to the open states pass through intermediate states, and Scheme XIII has closed states beyond the activation pathway. Schemes XII and XIII were examined because BK channels gate with large numbers of brief closings (flickers) at high $Ca^{2+}{}_i$, just as they do at lower $Ca^{2+}{}_i$ (Figs. 1, 3, and 6). Intermediate and/or secondary states are associated with the generation of flickers at lower $Ca^{2+}{}_i$ (Rothberg and Magleby, 1998). Additional support for possible intermediate closed states between the closed and open states comes from the observation of Cui et al. (1997) that there is a 50–150-μs delay in the activation of BK channels by voltage steps. Indirect support for possible secondary closed states comes from observations on *Shaker* K^+ channels, where secondary states appear to contribute to the gating (Hoshi et al., 1994; Zagotta et al., 1994; Schoppa and Sigworth, 1998). Homology between *Shaker* channels and the core region of BK channels (Wei et al., 1994; Toro et al., 1998) then suggests the possibility of considering such secondary states for BK channels.

Schemes XI–XIII were fitted to the 2-D dwell-time distributions obtained at a single high $Ca^{2+}{}_i$ of 1,024 μM for each of three channels. All three of these schemes gave reasonable descriptions of the kinetic structure at high $Ca^{2+}{}_i$ (not shown, but slightly better vi-

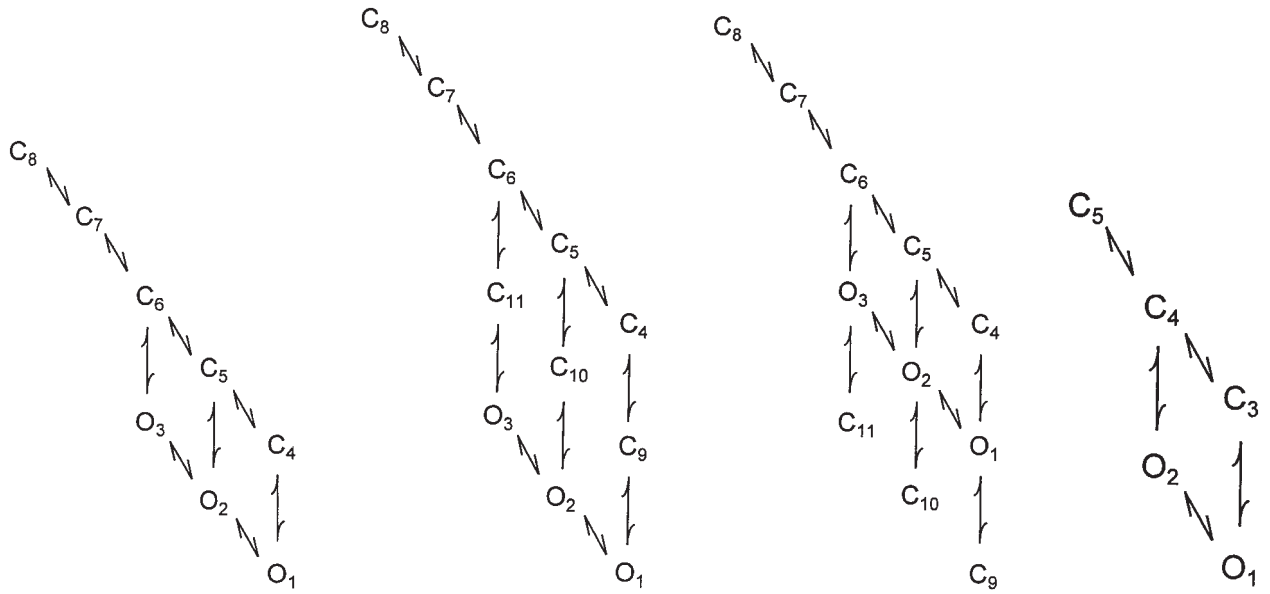

sually when compared with the experimental data than that shown in Fig. 10, D and H), and all three schemes gave detected numbers of open and closed states within the range observed in the experimental data at high Ca^{2+}_i. Scheme XI gave three open and four closed components, and Schemes XII and XIII each gave three open and five closed components. For purposes of comparison, a simpler Scheme XIV with only two open and three closed states, which describes the fully liganded states in Scheme X, was also examined.

Both the NLR_{1000} and Akaike criteria ranked the schemes in the order: Scheme XII $\sim$ Scheme XIII $>$ Scheme XI $>>$ Scheme XIV (Table IV). The likelihood ratio test was applied to the nested Schemes XIII, XI, and XIV, and gave highly significant ($P < 0.001$) rankings of: Scheme XIII $>$ Scheme XI $>$ Scheme XIV.

The values of the NLR_{1000} for Schemes XI, XII, and XIII (Table IV) indicated that the fits given by these schemes were considerably better than for the simpler Scheme XIV, and approached the theoretical best descriptions of the single data sets for discrete state Markov models. The values of the NLR_{1000} for these schemes ranged from 0.061 to 0.959, giving likelihood ratios per interval pair ranging from 0.9972 ($0.061^{0.001}$) to 0.9999 ($0.899^{0.001}$), suggesting little difference in likelihood per interval pair between the observed and theoretical best descriptions of the data.

These findings indicate that the gating of BK channels at high Ca^{2+}_i can be approximated by models based on the fully liganded states in Scheme IX. Scheme XI was drawn from the fully liganded states in Scheme IX. Adding three additional brief states as either intermediate states (Scheme XII) or secondary states (Scheme XIII) to generate additional flickers significantly improved the description of the data (Table IV). Whether the intermediate or secondary states are needed, or whether these additional states simply provide a means to compensate for the fact that fitting only the fully liganded states excludes potential contributions to the gating from transitions back to the states with fewer than four bound Ca^{2+} is not yet clear. What is clear, however, is that at least three open and five to eight closed states, as described by Schemes XI–XIII, are required to describe the gating at high Ca^{2+}_i equivalent to the theoretical best description. These schemes lack Ca^{2+}-dependent rate constants and apply only for $Ca^{2+}_i > \sim 100$ μM, where the gating kinetics are little affected by Ca^{2+}_i.

TABLE IV

Normalized Likelihood Ratios (NLR_{1000}) and Rankings (R) of Schemes XI–XIV Fitted to Data Obtained at 1,024 μM Ca^{2+}_i

	Channel 1 (B06)		Channel 2 (B12)		Channel 3 (B14)	
Scheme	NLR_{1000}	R	NLR_{1000}	R	NLR_{1000}	R
XIV	2.11 ± 10^{-4}	4	2.24 ± 10^{-5}	4	1.00×10^{-3}	4
XI	0.0610	3	0.117	3	0.238	3
XIII	0.468	2	0.950	2	0.828	2
XII	0.475	1	0.959	1	0.899	1

Scheme V with an Assumption of Saturation in the Ca^{2+}-dependent Rate Constants Could Approximate the Gating from Low to High Ca^{2+}_i

We also explored an alternative explanation to account for the lack of effect of Ca^{2+}_i on the gating at high Ca^{2+}_i. In all of the above considered schemes, the binding rate of Ca^{2+}_i was assumed to be a first order reaction, increasing linearly with Ca^{2+}_i. Thus, the effective rate constants for binding are given by the product of Ca^{2+}_i times the rate constants expressed per micromole per second. An upper limit for the rate constant for such a diffusion-controlled process is $\sim 10^9$ M^{-1} s^{-1} (Fersht, 1985; Cui et al., 1997). There is, however, no a priori reason to think that the effective binding rate would necessarily increase linearly with Ca^{2+}_i at high Ca^{2+}_i. The physical structure of the Ca^{2+}-binding sites is not yet known, but if the binding sites are in a vestibule with some additional negative charged groups, then the local concentration of Ca^{2+} at the binding sites at lower Ca^{2+} could be greater than that in the bulk solution (Van der Kloot and Cohen, 1979; Green and Andersen, 1991; Nonner and Eisenberg, 1998), so that the local concentration could reach a maximum as the concentration of Ca^{2+} in the bulk solution is raised. This could give an apparent saturation in the Ca^{2+}-dependent rate constants.

Alternatively, if the binding, which is represented by a one-step process in the kinetic schemes, is actually a two-step process that involves binding followed by a conformational change, then the apparent binding rate would saturate if the second step becomes rate limiting at high Ca^{2+}_i (Fersht, 1985).

Since the physical details involving Ca^{2+} binding and action are not known, we explored these two saturation models by using an approach that was independent of a detailed physical model. As both processes would have the effect of reducing the effective concentration of Ca^{2+}_i at high Ca^{2+}_i, we examined whether the kinetic structure from low to high Ca^{2+}_i could be described by letting the effective Ca^{2+}_i at high Ca^{2+}_i be less than the actual Ca^{2+}_i, to mimic apparent saturation of the binding step. Since it is not known what the value of the effective Ca^{2+}_i would be at high Ca^{2+}_i, this value was estimated by iterative fitting. The 2-D dwell-time distributions obtained at six different Ca^{2+}_i (5.5, 8.3, 12.3, 20.3, 132, and 1,024 μM) were simultaneously fitted to estimate the most likely rate constants for Scheme V, and also the most likely effective concentrations of Ca^{2+}_i for the data obtained at 132 and 1,024 μM Ca^{2+}_i. When fitting, the Ca^{2+}_i used for the data obtained at the four lower Ca^{2+}_i was fixed to the experimental values.

Scheme V with effective Ca^{2+}_i of 56.9 and 60.0 μM for the data obtained at 132 and 1,024 μM Ca^{2+}_i, respectively, and the actual Ca^{2+}_i for the other four data sets obtained at lower Ca^{2+}_i could approximate the basic features of the kinetic structure from low to high Ca^{2+}_i. The predicted kinetic structure at 1,024 μM Ca^{2+}_i is shown in Fig. 11 and was visually indistinguishable from the predicted kinetic structure at 132 μM Ca^{2+}_i. Comparison of the predicted kinetic structure in Fig. 11 to that in Fig. 6, C, D, G, and H, showed that Scheme V with an assumption of saturation could approximate the data at high Ca^{2+}_i. Scheme V with saturation also described the data at lower Ca^{2+}_i, with the predicted structure similar to that in Fig. 10 (not shown). For the other two channels studied in a similar manner, the effective Ca^{2+}_is at 132 and 1,024 μM Ca^{2+}_i were 67.8 and 114 μM (channel B12) and 35.2 and 39.4 μM (channel B14). The likelihoods indicated that Scheme V with an effective saturation in the binding rate (Scheme V-sat) described the kinetic structure from low to high Ca^{2+}_i slightly less well than Schemes VII and X (Table III). The observation that the effective Ca^{2+}_i was greater for all three channels for the data collected at 1,024 μM than for the data collected at 132 μM suggests that increasing Ca^{2+}_i from 132 to 1,024 μM may have some additional effects on the gating, but any effects would be small since the exponential components describing the dwell-time distributions at 132 and 1,024 μM Ca^{2+}_i were not significantly different. Cox et al. (1997b) have also found (for *mSlo*) that high Ca^{2+}_i may have additional effects on gating.

The results in this section show that a relatively simple gating mechanism (Scheme V) with the added assumption of apparent saturation in the Ca^{2+} binding steps at high Ca^{2+}_i can approximate the gating from low to high Ca^{2+}_i. It will be discussed later that saturating models may be less appropriate than two-tiered models.

Estimated Rate Constants for the Examined Kinetic Schemes

Fig. 12 presents the estimated rate constants for Schemes X and XI for the three channels examined in detail. Online supplemental Figure S2 (http://www.jgp.org/cgi/full/114/1/93/DC1) presents estimated rate constants for these same three channels for most of the other examined schemes. The rate constants for the examined schemes typically ranged from ~0 to 45,000/s, indicating a large range in the height of the energy barriers between the various states. Rate constants were limited so as not to exceed 45,000/s, as letting them go higher gave little improvement in the fits. Estimated rate constants for the simpler models (Schemes IV–VI and XI–XIII) were relatively consistent from channel to channel. For the most complex gating mechanism examined (Scheme X), there could be considerable variability in the estimates, depending on the specific rate constants. In those cases where there was considerable variability in estimates of the rate constants among channels, the variability was typically associated with poorly defined rate constants, as these rate constants could be fixed to various values with little effect on the likelihood values after refitting. The rate constants for Scheme X will be used in the discussion to describe how the channel gates at low and high Ca^{2+}.

discussion

This study used detailed single-channel analysis to examine the Ca^{2+}-dependent gating of native BK channels in cultured rat skeletal muscle. We have extended previous studies by examining the effects of high Ca^{2+}_i to obtain critical information about mechanism when the gating is driven towards the fully liganded states. Maximum likelihood fitting together with comparisons of the observed and predicted 2-D dwell-time distributions and dependency plots (the kinetic structure) were used to evaluate gating mechanisms.

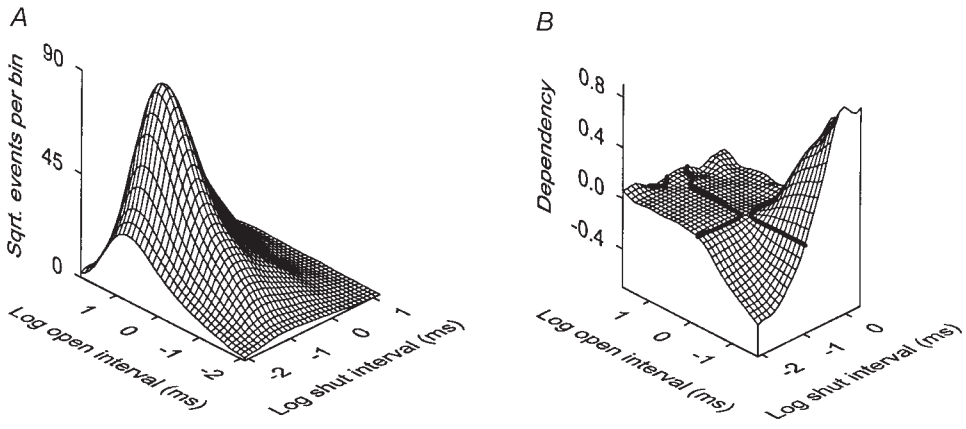

Figure 11. Scheme V with an assumption of saturation in the Ca^{2+}-binding rates (Scheme V-sat in Table III) describes the kinetic structure from low to high Ca^{2+}_i. The figure presents the predicted kinetic structure for data obtained with 1,024 μM Ca^{2+}_i (compare with Fig. 6, D and H). The rate constants used in the predictions were obtained by simultaneous maximum likelihood fitting of 2-D distributions obtained at six different Ca^{2+}_i ranging from 5.5 to 1,024 μM. The values of the effective Ca^{2+} at the binding sites for the data obtained at 132 and 1,024 μM Ca^{2+}_i were determined by fitting to maximize the likelihood during the simultaneous fitting of data obtained at the six different Ca^{2+}_i, and were 56.9 and 60.0 μM Ca^{2+}_i, respectively. Channel B06. The predicted kinetic structure for 132 μM Ca^{2+}_i was similar to that plotted in A and B, and the predicted kinetic structures for the lower Ca^{2+}_i were similar to those shown in Fig. 10.

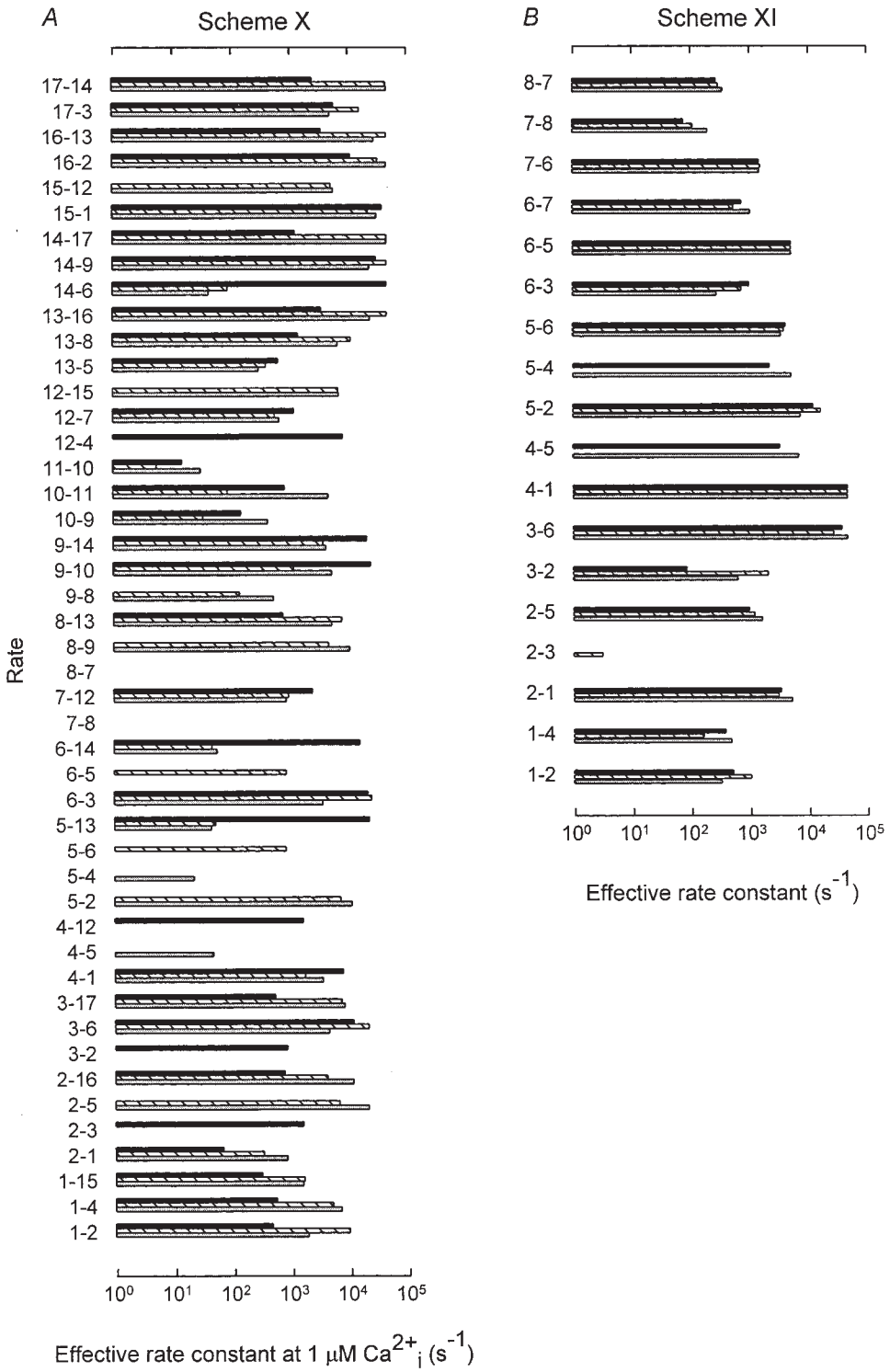

Figure 12. Estimated rate constants for Schemes X and XI for three BK channels. B06 (black bar), B12 (hatched bar), and B14 (light gray bar). Rate constants in A were estimated by the simultaneous fitting of 2-D dwell-time distributions at six different Ca^{2+}_i. Rate constants in B were estimated by the fitting of the 2-D dwell-time distributions obtained at 1,024 μM Ca^{2+}_i only. (Rate constants for other examined schemes can be found in online supplemental Figure S2 [http://www.jgp.org/cgi/full/114/1/93/DC1].)

Properties of Gating in High Ca^{2+}_i

For low to intermediate levels of Ca^{2+}_i, the gating was highly Ca^{2+}_i dependent, with a Hill coefficient of ~3.5, within the range of 2–4 typically observed for BK channels (see introduction). In contrast, the gating was Ca^{2+} independent for high levels of Ca^{2+}_i (>100 μM). Increasing Ca^{2+}_i 8–10-fold to 1,024 μM had little effect on P_o (~0.97), the mean open and closed times, the 1- and 2-D dwell-time distributions, and the dependency plots (Figs. 1–4, 6–8, and Tables I and II). Estimates of the numbers of significant exponential components in the dwell-time distributions indicated that the channel entered at least three to four open and four to five closed states during normal activity at high Ca^{2+}_i, and

that the estimated numbers of states did not change when Ca^{2+}_i was increased from 100 to 1,024 μM (Fig. 4). Significant dependencies (correlations) between the durations of adjacent open and closed intervals in the dependency plots (Figs. 6–8) indicated that transitions between the open and closed states occurred over at least two independent transition pathways (two or more gateway states) at high Ca^{2+}_i.

Thus, as a first approximation, gating at high Ca^{2+}_i involves Ca^{2+}-independent transitions among at least three to four open and four to five closed states, with two or more independent transition pathways among the open and closed states. Models with these characteristics (Schemes XI–XIII) gave excellent descriptions of the kinetic structure for data limited to high Ca^{2+}_i (Table IV).

The MWC Model Is Inconsistent With Gating from Low through High Ca^{2+}_i

The MWC model (Monod et al., 1965) for allosteric proteins (Scheme III) predicts that high Ca^{2+}_i would drive the gating towards the two fully liganded open and closed states, resulting in a simple two-state gating mechanism at high Ca^{2+}_i with a single transition pathway between the states. These predictions of the MWC model are inconsistent with our observations at high Ca^{2+}_i of multiple open and closed states connected by two or more independent transition pathways. The MWC model or extensions of the MWC model (Schemes IV–VI) could not describe the gating from low to high Ca^{2+}_i (Fig. 5 and Table III). Clearly, the MWC model can be rejected for the gating of BK channels in skeletal muscle.

Models with a Single Effective Gateway State at High Ca^{2+}_i Can Be Rejected

Since models based on the MWC model were inconsistent with the data at high Ca^{2+}_i, we examined more complex models based on Eigen's (1968) general 35-state allosteric model for tetrameric proteins and the 55-state extension of Eigen's model (Cox et al., 1997a) shown in Scheme I. Since both the 35- and the 55-state models have too many rate constants to estimate practically, we condensed these models to a 25-state model (Scheme II) by assuming that the isoforms of each state were kinetically indistinguishable (as in Fersht, 1985), and then examined models drawn from the 25-state model. Scheme VII could describe the 1-D dwell-time distributions from low to high Ca^{2+}_i (Fig. 5), but predicted no dependence between adjacent intervals at high Ca^{2+}_i (Fig. 9), in contrast to the significant dependencies observed in the experimental data (Figs. 6–8).

The lack of dependence for Scheme VII at high Ca^{2+}_i results because the high Ca^{2+}_i drives the gating towards the fully liganded states, as summarized by Scheme VIII, where there is a single effective transition pathway between the open and closed states. The observation that Scheme VII predicted no dependence at high Ca^{2+}_i suggests by analogy that the more complex 25–55-state models (Schemes I and II), and all schemes in which there would be a single effective transition pathway between open and closed states at high Ca^{2+}_i, can be rejected.

A General Two-Tiered Model Can Account for the Gating from Low to High Ca^{2+}_i

Schemes I–VII can be classified as one tiered because the open and closed states can be contained within a single plane. Since the examined one-tiered models were inadequate to describe the data at high Ca^{2+}_i, we considered what type of model would be required. If all the states in Schemes I and II are closed states, then there would be a sufficient number of fully liganded closed states at high Ca^{2+} to generate the four to five observed closed exponential components observed at high Ca^{2+}. If each of the closed states in Schemes I and II can make a direct transition to an open state, then this would give enough fully liganded open states to generate the three to four observed open components at high Ca^{2+}. If the gating is effectively confined to the fully liganded states at high Ca^{2+}_i, then the gating at high Ca^{2+}_i would be described by Scheme XV, where all the subunits are bound with Ca^{2+}. Each subunit in this scheme can exist in two conformational states, and a concerted conformational change of all subunits is required for opening. Scheme XV has five independent transition pathways between the fully liganded closed and open states (upper and lower tiers, respectively) that would allow dependence to be generated between open and closed intervals at high Ca^{2+}_i. Scheme XI, consistent with Scheme XV, gave excellent descriptions of the gating in high Ca^{2+}_i (Table IV)

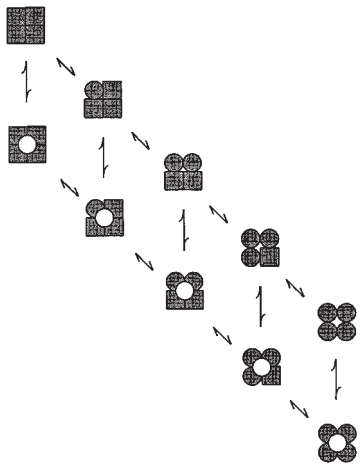

(scheme xv)

Extending Scheme XV to include states with zero to three bound Ca^{2+} would give the general two-tiered model described by Scheme IX, with 25 closed states on the upper tier and 25 open states on the lower tier. Scheme X, a reduced version of Scheme IX, could describe the kinetic structure of the channel from low to high Ca^{2+}_i (Fig. 10). Scheme X also generated single-channel current records that closely mimicked, except for stochastic variation, the experimental current records, as can be seen by comparing the simulated (predicted) records in Fig. 13 to the experimental records in Fig. 1. The Ca^{2+}-independent gating kinetics at high Ca^{2+}_i together with the few longer closed intervals are present in the simulated records.

Although the more complex Scheme IX was not tested directly, this general scheme should give an even better description of the gating than Scheme X, as Scheme X is contained within Scheme IX. Hence, Scheme IX can serve as a working hypothesis for the Ca^{2+}-dependent gating of BK channels. Horrigan and Aldrich (personal communication), based on analysis of macroscopic ionic and gating currents from *mSlo*, have also found evidence for two-tiered gating mechanisms.

Gating in Scheme IX Occurs Among Five Subschemes that Differ in the Number of Bound Ca^{2+}

In the context of Scheme IX, it can be seen that, for any fixed number (0–4) of Ca^{2+} bound to the channel, the channel could gate among at least five open and five closed states. Thus, Scheme IX can be viewed as being comprised of five subschemes (one of which is shown in Scheme XV). The subunit conformations of the analogous states in each of the subschemes are the same, as are the transition pathways among the various open and closed states. Hence, both the conformations of the subunits and the connections among states are identical for each subscheme, independent of the number of bound Ca. Ca^{2+}_i acts by driving the gating from the subscheme comprised of the states with zero bound Ca^{2+} towards the subscheme comprised of the states with four bound Ca^{2+}. The binding of Ca^{2+} stabilizes the open states. The dynamics of this Ca^{2+}-dependent shift will be presented in a later section.

Additional support for Scheme IX comes from the observation that BK channels gate at very low Ca^{2+}_i (Barrett et al., 1982; Pallotta, 1985; Meera et al., 1996; Rothberg and Magleby, 1996; Cui et al., 1997), among multiple closed (Talukder and Aldrich, 1998) and open states (Nimigean, Rothberg, and Magleby, unpublished observations). The unliganded states in Scheme IX have five gateway states, suggesting that there would be a dependent relationship among the durations of open and closed intervals at zero Ca^{2+}_i, consistent with unpublished observations (Nimigean, Rothberg, and Magleby).

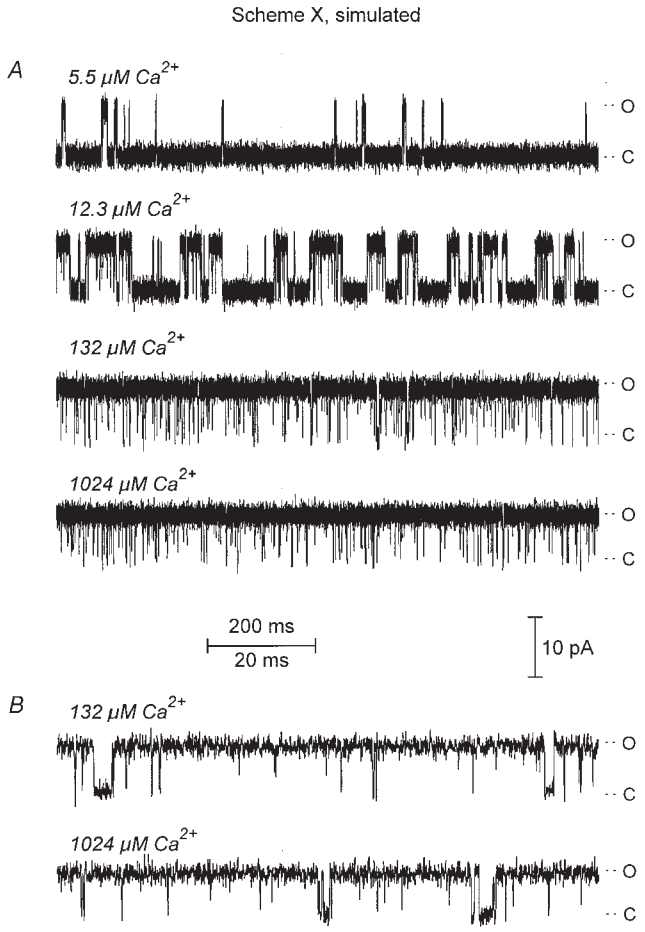

Figure 13. Single-channel current records predicted by the two-tiered Scheme X for comparison with the experimental current records in Fig. 1. Idealized single-channel currents were generated, noise was added, and then the entire record was filtered with a digital four-pole Bessel filter to give the same effective dead time as that in the experimental record. Scheme X predicts the range of activity as well as the apparent kinetic saturation in the gating at high Ca^{2+}_i.

Why the Dependency Plots Appear Similar from Low to High Ca^{2+}_i

The saddle shape of the dependency plots (Figs. 6 and 7) reflects the inverse relationship between the durations of adjacent open and closed intervals. This inverse relationship suggests that more stable (longer duration) open states are effectively connected to less stable (briefer duration) closed states (McManus et al., 1985). In terms of Scheme IX, the general saddle shape of the dependency plots remains the same from low through high Ca^{2+}_i because the subschemes that are entered from low to high Ca^{2+}_i are comprised of the same numbers of open and closed states with the same subunit conformations and connections among the states. If the relative stability of the connected open and closed states depends mainly on the subunit con-

formations rather than on the numbers of bound Ca^{2+}_i, then the general shape of the dependency plots would remain the same from low through high Ca^{2+}_i.

Gating Dynamics at Low and High Ca^{2+}_i

Since Scheme X (drawn from Scheme IX) could account for the kinetic structure from low to high Ca^{2+}_i, Scheme X was examined to gain insight into how Ca^{2+} activates the channel. Fig. 14 presents the equilibrium occupancy, mean lifetime, and frequency of entry for each state for gating at low Ca^{2+}_i (5.5 μM, P_o = 0.061) and high Ca^{2+}_i (1,024 μM, P_o = 0.97) for Scheme X. Notice that bars of considerable height in these plots can have small values due to the logarithmic ordinates.

At low Ca^{2+}_i (Fig. 14, A–C), the channel readily gates among all of the states in Scheme X, as indicated by the frequencies of entry into each state (C), but spends most of its time in the closed states with zero (82.9%) and one (8.2%) bound Ca^{2+}_i (A). At high Ca^{2+}_i, the gating of the channel is effectively confined to the fully liganded states with four bound Ca^{2+}, where it spends 99.2% of its time. Little time (0.76%) is spent in the states with three bound Ca^{2+}, and negligible time (<0.04%) is spent in the states with 0, 1, or 2 bound Ca^{2+}_i (Fig. 14, D–F). The high P_o in high Ca^{2+} reflects that the channel spends 96.6% of its time in the open states with four bound Ca^{2+}, where Ca^{2+} stabilizes the open states. The flickers (brief closings) in the single-channel current record arise mainly from transitions to

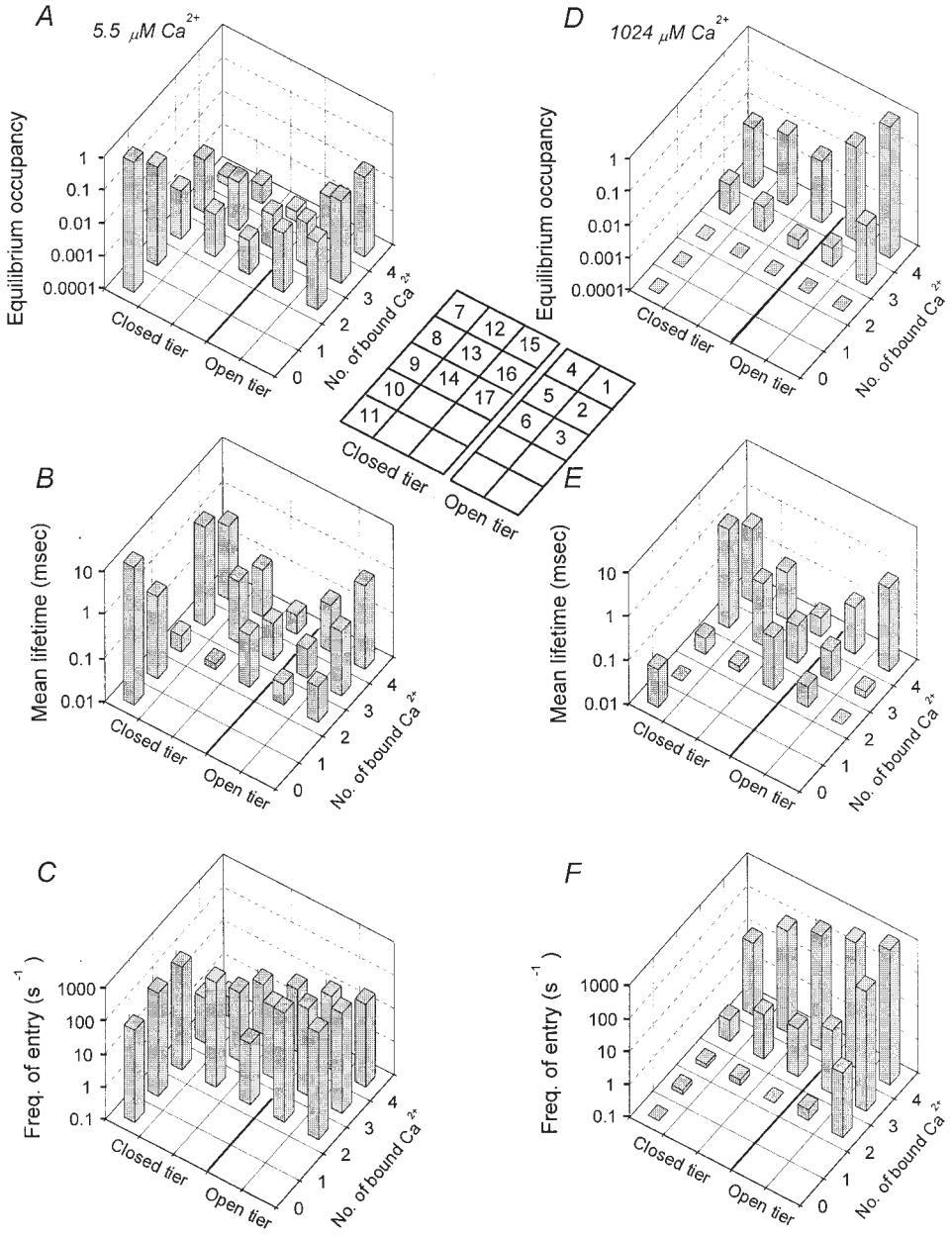

Figure 14. Mechanism of the Ca^{2+}-dependent gating of BK channels for the two-tiered model described by Scheme X. Equilibrium occupancies, mean lifetimes, and frequencies of entry into each state are plotted on logarithmic scales for data collected at low (A–C, 5.5 μM) and high (D–F, 1,024 μM) Ca^{2+}_i. The x axis indicates the number of bound Ca^{2+}, and the y axis indicates the upper tier of closed states and the lower tier of open states. The inset identifies the states in the plots with the state numbers in Scheme X. The two-tiered form of Scheme X places open states 1–3 directly below closed states 15–17, respectively, and open states 4–6 directly below closed states 12–14, respectively. Channel B06.

the brief closed states C12– C16 at lower Ca^{2+}_i and C12 and C15 at high Ca^{2+}_i.

The Considered Schemes Are Only Approximations of the Gating Mechanism

As emphasized by Schoppa and Sigworth (1998), all kinetic modeling is by nature approximate. Although Scheme X could give good descriptions of the single-channel kinetics from low to high Ca^{2+}_i, this model must be considered as only an approximation of the actual underlying gating mechanism. Scheme X with 17 states was drawn from the general 50-state model described by Scheme IX. Additional open and closed states with zero and one bound Ca^{2+}_i would have to be added to Scheme X to allow gating in very low Ca^{2+}_i, and additional rows of open and closed states would have to be added to Scheme X to generate the observed numbers of open and closed components at high Ca^{2+}_i. The addition of these states would bring Scheme X to the general 50-state model described by Scheme IX.

However, even the general 50-state Scheme IX is a reduced model compared with what the actual gating mechanism is likely to be. Scheme IX excludes the isoforms of the various open and closed states. Including all the isoforms of each state (see Scheme I) would expand Scheme IX from 50 to 110 states.

BK channels may have additional closed states beyond the activation pathway (secondary states). Rothberg and Magleby (1998) found that models with such secondary states were consistent with the gating from low to intermediate Ca^{2+}_i, and Scheme XIII with such secondary states gave excellent descriptions of gating in high Ca^{2+}_i (Table IV). Such secondary states, if present, would add a third tier to Schemes IX and X consisting of closed states beyond the open states. Secondary states may also contribute to the gating of other K^+ channels (Hoshi et al., 1994; Schoppa and Sigworth, 1998).

The skeletal muscle BK channel often passes through a brief lifetime subconductance state upon opening and closing (Ferguson et al., 1993). It is not clear whether these subconductance states would arise from some of the states in Schemes IX and X, from isoforms of the states (see Scheme I) that were not included in Schemes IX and X, or whether additional states would have to be added to Schemes IX and X to account for the subconductance levels. For example, the concerted conformational changes that occur between closing and opening may occur in two steps, rather than the one indicated in Schemes IX and X (Schoppa and Sigworth (1998).

Changing Ca^{2+}_i more than two orders of magnitude, as was done in our experiments, would be expected to alter surface charge (Hille et al., 1975; Green and Andersen, 1991) and hence gating (Moczydlowski et al., 1985). Since the considered gating mechanisms did not take surface charge into consideration, the question arises as to what effects this omission might have on the conclusions of our study. Changing the membrane potential $\pm$20 mV (to mimic possible surface charge effects) did not alter the observed numbers of exponential components or the general saddle shape of the dependency plots (our unpublished observations). Since the rejection of previous models in favor of two-tiered gating mechanisms in our study was based on factors that relate to the observed numbers of states and dependency at high Ca^{2+}_i, surface charge effects would be unlikely to alter the conclusion of two-tiered gating mechanisms reached in this study, but could alter some of the rate constants.

Although Scheme X could describe many features of the data, this does not exclude the possibility that other rather different mechanisms might also account for the data. A model with fewer states than Scheme X, but with apparent saturation in Ca^{2+} binding rate could also give reasonable descriptions of the Ca^{2+} dependence of the single-channel kinetics from low to high Ca^{2+}_i (Fig. 11 and Table III). Nevertheless, we prefer the general two-tiered approach based on Scheme IX to the more ad hoc saturation models, as two-tiered models provide a means to account for the complexity of the gating in zero Ca^{2+}_i and are consistent with a tetrameric protein.

BK channels can gate in a number of different modes, with 96% of the intervals occurring during activity in the normal mode (McManus and Magleby, 1988). The gating mechanisms developed in this study apply only to normal mode activity and would have to be expanded to account for activity in other modes. The gating mechanisms would also have to be expanded or modified to account for the effects of permeant ions on channel activity (Demo and Yellen, 1992; Mienville and Clay, 1996), the different gating properties of other BK channels such as *dSlo* (from Drosophila) where mean open times are relatively Ca^{2+} independent (Lagrutta et al., 1994; Moss et al., 1999), and the gating effects of various beta subunits not present in skeletal muscle (McManus et al., 1995; Dworetzky et al., 1996; Solaro et al., 1997; Tanaka et al., 1997; Nimigean and Magleby, 1999; Waller et al., 1999).

Voltage Dependence of Gating

The voltage dependence of BK channels is an intrinsic property of the channel and does not appear to arise through voltage-dependent increases in Ca^{2+} binding (Cox et al., 1997b; Cui et al. 1997; Rothberg and Magleby, 1996, 1999; Stefani et al., 1997; Diaz et al., 1998). BK channels show homology to the superfamily of voltage-dependent K^+ channels, including an S4 voltage

sensor (Atkinson et al., 1991; Adelman et al., 1992; Butler et al., 1993; Pallanck and Ganetzky, 1994; Diaz et al., 1998). In the context of the general two-tiered Scheme IX, depolarization could increase P_o through voltage-dependent transitions of two general types. Depolarization could drive the concerted conformational changes that occur when states on the closed tier open to states on the open tier, or depolarization could drive the conformational changes of the individual subunits for transitions among states on each tier.

Recent preliminary observations on large multistate models using analysis of macroscopic ionic and gating currents (Horrigan and Aldrich, 1998) and single-channel recordings (Rothberg and Magleby, unpublished observations) suggest that the voltage dependence lies mainly in the Ca^{2+}-independent closed–closed and open–open steps with the concerted closed–open step being less voltage dependent. Consistent with this hypothesis, gating charge movement can precede channel opening, and charge movement can also occur after the pore is open (Stefani et al., 1997). These observations suggest that it may only be necessary to add voltage dependence to the rate constants in the models that we have considered in order to account for the major features of the voltage dependence of the single-channel kinetics. Nevertheless, *Shaker* K^+ channels gate as if each subunit undergoes three transitions in sequence followed by two final concerted transitions for opening (Schoppa and Sigworth, 1998), and movement of the S2 segment may precede that of the S4 segment (Cha and Bezanilla, 1997), consistent with multiple conformations of each subunit. If the subunits in BK channels also have multiple conformations, then the potential numbers of states would be greatly increased over the models considered here.

Conclusion

This study develops gating mechanisms that can describe the Ca^{2+} dependence of the kinetic structure of BK channels from low to kinetically saturating levels of Ca^{2+}_i. These models are drawn from a general 50-state two-tiered model in which each closed state in the upper tier can make a direct transition to an open state in the lower tier. Our previous models that describe the Ca^{2+}-dependent gating over more limited conditions are contained within the general 50-state model. Thus, the 50-state model serves to unify previous studies, and can provide a framework for further studies on mechanism through single-channel analysis of gating at very low Ca^{2+}_i and of the voltage dependence of the gating.

This work was supported in part by grants from the National Institutes of Health (NS007044 and AR32805) and the Muscular Dystrophy Association.

Submitted: 5 March 1999 Revised: 6 May 1999 Accepted: 7 May 1999

Note added in Proof. Forthcoming kinetic studies lend additional support to Scheme IX. Gating currents and macroscopic ionic currents recorded from m*Slo* BK channels in the absence of Ca^{2+} are consistent with a model that is described by the unliganded states in Scheme IX. (Horrigan, F.T., J. Cui, and R.W. Aldrich. 1999. Allosteric voltage-gating of potassium channels I: m*Slo* ionic currents in the absence of Ca^{2+}. *J. Gen. Physiol.* In press. Horrigan, F.T., and R.W. Aldrich. 1999. Allosteric voltage-gating of potassium channels II: m*Slo* channel gating charge movement in the absence of Ca^{2+}. *J. Gen. Physiol*. In press.)

references

Adelman, J.P., E. Shen, M.P. Kavanaugh, R.A. Warren, Y. Wu, A. Lagrutta, C. Bond, and R.A. North. 1992. Calcium-activated potassium channels expressed from cloned complementary DNAs. *Neuron*. 9:209–216.

Akaike, H. 1974. A new look at the statistical model identification. *IEEE (Inst. Electr. Electron. Eng.) Trans. Auto. Control*. 19:716–723.

Art, J.J., Y.-C. Wu, and R. Fettiplace. 1995. The calcium-activated potassium channels of turtle hair cells. *J. Gen. Physiol*. 105:49–72.

Atkinson, N.S., G.A. Robertson, and B. Ganetzky. 1991. A component of calcium-activated potassium channels encoded by the *Drosophila slo* locus. *Science.* 253:551–555.

Barrett, J.N., K.L. Magleby, and B.S. Pallotta. 1982. Properties of single calcium-activated potassium channels in cultured rat muscle. *J. Physiol.* 331:211–230.

Bauer, R.J., B.F. Bowman, and J.L. Kenyon. 1987. Theory of the kinetic analysis of patch clamp data. *Biophys. J.* 52: 961–978.

Bello, R.A., and K.L. Magleby. 1998. Time-irreversible subconductance gating coupled to permeation of Ba^{2+} through large-conductance Ca^{2+}-activated K^+ channels. *J. Gen. Physiol.* 111: 343–362.

Bezanilla, F., E. Perozo, and E. Stefani. 1994. Gating of *Shaker* K^+ channels: II. The components of gating currents and a model of channel activation. *Biophys. J.* 66:1011–1021.

Blatz, A.L., and K.L. Magleby. 1986. Correcting single channel data for missed events. *Biophys. J.* 49:967–980.

Butler, A., S. Tsunoda, D.P. McCobb, A. Wei, and L. Salkoff. 1993. mSlo, a complex mouse gene encoding "maxi" calcium-activated potassium channels. *Science.* 261:221–224.

Cha, A., and F. Bezanilla. 1997. Characterizing voltage-dependent conformational changes in the *Shaker* K^+ channel with fluorescence. *Neuron*. 19:1127–1140.

Chang, C.-P., S.I. Dworetzky, J. Wang, and M.E. Goldstein. 1997. Differential expression of the α and β subunits of the large-conductance calcium-activated potassium channel: implication for channel diversity. *Mol. Brain Res.* 45:33–40.

Colquhoun, D. 1973. The relation between classical and coopera-

tive models for drug action. *In* Drug Receptors. H.P. Rang, editor. University Park Press, London. 149–182.

Colquhoun, D., and A.G. Hawkes. 1981. On the stochastic properties of single ion channels. *Proc. R. Soc. Lond. B Biol. Sci.* 211:205–235.

Colquhoun, D., and A.G. Hawkes. 1987. A note on correlations in single ion channel records. *Proc. R. Soc. Lond. B Biol. Sci.* 230: 15–52.

Colquhoun, D., and A.G. Hawkes. 1995a. The principles of the stochastic interpretation of ion-channel mechanisms. *In* Single-Channel Recording. B. Sakmann and E. Neher, editors. Plenum Publishing Corp., New York. 397–482.

Colquhoun, D., and A.G. Hawkes. 1995b. A Q-matrix cookbook. *In* Single-Channel Recording. B. Sakmann and E. Neher, editors. Plenum Publishing Corp., New York. 589–633.

Colquhoun, D., and F.J. Sigworth. 1995. Fitting and statistical analysis of single-channel records. *In* Single-Channel Recording. B. Sakmann and E. Neher, editors. Plenum Publishing Corp., New York. 483–587.

Conley, E.C. 1996. The ion channel facts book. II. Intracellular ligand-gated channels. Academic Press, New York. 607–720.

Crouzy, S.C., and F.J. Sigworth. 1990. Yet another approach to the dwell-time omission problem of single-channel analysis. *Biophys. J.* 58:731–743.

Cox, D.H., J. Cui, and R.W. Aldrich. 1997a. Separation of gating properties from permeation and block in *mslo* large conductance Ca-activated K^+ channels. *J. Gen. Physiol.* 109:633–646.

Cox, D.H., J. Cui, and R.W. Aldrich. 1997b. Allosteric gating of a large conductance Ca-activated K^+ channel. *J. Gen. Physiol.* 110: 257–281.

Cui, J., D.H. Cox, and R.W. Aldrich. 1997. Intrinsic voltage dependence and Ca^{2+} regulation of *mslo* large conductance Ca-activated K^+ channels. *J. Gen. Physiol.* 109:647–673.

Demo, S.D., and G. Yellen. 1992. Ion effects on gating of the Ca^{2+}-activated K^+ channel correlates with occupancy of the pore. *Biophys. J.* 61:639–648.

Diaz, L., P. Meera, J. Amigo, E. Stefani, O. Alvarez, L. Toro, and R. Latorre. 1998. Role of the S4 segment in a voltage-dependent calcium-sensitive potassium (h*Slo*) channel. *J. Biol. Chem.* 273: 32430–32436.

DiChiara, T.J., and P.H. Reinhart. 1995. Distinct effects of Ca^{2+} and voltage on the activation and deactivation of cloned Ca^{2+}-activated K^+ channels. *J. Physiol.* 489:403–418.

Dworetzky, S.I., C.G. Boissard, J.T. Lum-Ragan, M.C. McKay, D.J. Post-Munson, J.T. Trojnacki, C.-P. Chang, and V.K. Gribkoff. 1996. Phenotypic alteration of a human BK (*hSlo*) channel by *hSlo*β subunit coexpression: changes in blocker sensitivity, activation/relaxation and inactivation kinetics, and protein kinase A modulation. *J. Neurosci.* 16:4543–4550.

Eigen, M. 1968. New looks and outlooks on physical enzymology. *Q. Rev. Biophys.* 1:3–33.

Ferguson, W.B. 1991. Competitive Mg^{2+} block of a large-conductance Ca^{2+}-activated K^+ channel in rat skeletal muscle. *J. Gen. Physiol.* 98:163–181.

Ferguson, W.B., O.B. McManus, and K.L. Magleby. 1993. Opening and closing transitions for BK channels often occur in two steps via sojourns through a brief lifetime subconductance state. *Biophys. J.* 65:702–714.

Fersht, A. 1985. Enzyme Structure and Mechanism. W.H. Freeman Co., San Francisco, CA. 263–278.

Fredkin, D.R., M. Montal, and J.A. Rice. 1985. Identification of aggregated Markovian models: application to the nicotinic acetylcholine receptor. *In* Proceedings of the Berkeley Conference in Honor of Jerzy Neyman and Jack Kiefer. L.M. LeCam, and R.A. Olshen, editors. Wadsworth Publishing Co., Belmont, CA. 269–289.

Golowasch, J., A. Kirkwood, and C. Miller. 1986. Allosteric effects of Mg^{2+} on the gating of Ca^{2+}-activated K^+ channels from mammalian skeletal muscle. *J. Exp. Biol.* 124:5–13.

Green, W.N., and O.S. Andersen. 1991. Surface charges and ion channel function. *Annu. Rev. Physiol.* 53:341–359.

Hamill, O.P., A. Marty, E. Neher, B. Sakmann, and F.J. Sigworth. 1981. Improved patch clamp techniques for high-resolution current recording from cells and cell-free membrane patches. *Pflügers Arch.* 391:85–100.

Hawkes, A.G., A. Jalali, and D. Colquhoun. 1992. Asymptotic distributions of apparent open times and shut times in a single channel record allowing for the omission of brief events. *Philos. Trans. R. Soc. Lond. B Biol. Sci.* 337:383–404.

Hille, B., A.M. Woodhull, and B.I. Shapiro. 1975. Negative surface charge near sodium channels of nerve: divalent ions, monovalent ions, and pH. *Phil. Trans. R. Soc. Lond. B Biol. Sci.* 170: 301–318.

Horn, R. 1987. Statistical methods for model discrimination: application to gating kinetics and permeation of the acetylcholine receptor channel. *Biophys. J.* 51:255–263.

Horn, R., and K. Lange. 1983. Estimating kinetic constants from single channel data. *Biophys. J.* 43:207–223.

Horrigan, F.T., and R.W. Aldrich. 1998. Allosteric voltage-gating and the effects of calcium on mslo Ca^{2+}-activated K^+ channels. *Biophys. J.* 74:A218.

Hoshi, T., W.N. Zagotta, and R.W. Aldrich. 1994. *Shaker* potassium channel gating. I: Transitions near the open state. *J. Gen. Physiol.* 103:249–278.

Kienker, P. 1989. Equivalence of aggregated Markov models of ion-channel gating. *Proc. R. Soc. Lond. B Biol. Sci.* 236:269–309.

Lagrutta, A., K.R.A. Shen, R.A. North, and J.P. Adelman. 1994. Functional differences among alternatively spliced variants of *slowpoke*, a *Drosophila* calcium-activated potassium channel. *J. Biol. Chem.* 269:20347–203511.

Latorre, R. 1994. Molecular workings of large conductance (maxi) Ca^{2+} -activated K^+ channels. *In* Handbook of Membrane Channels: Molecular and Cellular Physiology. C. Peracchia, editor. Academic Press, Inc., New York. 79–102.

Magleby, K.L. 1992. Preventing artifacts and reducing errors in single-channel analysis. *Methods Enzymol.* 207:763–791.

Magleby, K.L., and B.S. Pallotta. 1983. Burst kinetics of single calcium-activated potassium channels in cultured rat skeletal muscle. *J. Physiol.* 344:605–623.

Magleby, K.L., and L. Song. 1992. Dependency plots suggest the kinetic structure of ion channels. *Proc. R. Soc. Lond. B Biol. Sci.* 249: 133–142.

Magleby, K.L., and D.S. Weiss. 1990a. Estimating kinetic parameters for single channels with simulation. A general method that resolves the missed event problem and accounts for noise. *Biophys. J.* 58:1411–1426.

Magleby, K.L., and D.S. Weiss. 1990b. Identifying kinetic gating mechanisms for ion channels by using two-dimensional distributions of simulated dwell times. *Proc. R. Soc. Lond. B Biol. Sci.* 241: 220–228.

Marty, A. 1989. The physiological role of calcium-dependent channels. *Trends Neurosci.* 12:420–424.

McManus, O.B. 1991. Calcium-activated potassium channels: regulation by calcium. *J. Bioenerg. Biomembr.* 23:537–560.

McManus, O.B., A.L. Blatz, and K.L. Magleby. 1985. Inverse relationship of the durations of adjacent open and shut intervals for Cl and K channels. *Nature.* 317:625–628.

McManus, O.B., A.L. Blatz, and K.L. Magleby. 1987. Sampling, log binning, fitting, and plotting durations of open and shut intervals from single channels and the effects of noise. *Pflügers Arch.* 410:530–553.

McManus, O.B., L.M.H. Helms, L. Pallanck, B. Ganetzky, R. Swanson, and R.J. Leonard. 1995. Functional role of the beta subunit of high-conductance calcium-activated potassium channels. *Neuron*. 14:645–650.

McManus, O.B., and K.L. Magleby. 1988. Kinetic states and modes of single large-conductance calcium-activated potassium channels in cultured rat skeletal muscle. *J. Physiol*. 402:79–120.

McManus, O.B., and K.L. Magleby. 1989. Kinetic time constants independent of previous single-channel activity suggest Markov gating for a large-conductance Ca-activated K channel. *J. Gen. Physiol*. 94:1037–1070.

McManus, O.B., and K.L. Magleby. 1991. Accounting for the Ca^{2+}-dependent kinetics of single large-conductance Ca^{2+}-activated K^+ channels in rat skeletal muscle. *J. Physiol*. 443:739–777.

Meera, P., M. Wallner, Z. Jiang, and L. Toro. 1996. A calcium switch for the functional coupling between α (*hslo*) and β subunits (K_α, Caβ) of maxi K channels. *FEBS Lett.* 382:84–88.

Mendenhall, W., R.L. Scheaffer, and D.D. Wackerly. 1990. Mathematical statistics with applications. PWS-Kent Publishing Co., Boston. 650–655.

Mienville, J.-M., and J.R. Clay. 1996. Effects of intracellular K^+ and Rb^+ on gating of embryonic rat telencephalon Ca^{2+}-activated K^+ channels. *Biophys. J.* 70:778–785.

Miller, C. 1987. Trapping single ions inside single ion channels. *Biophys. J.* 52:123–126.

Moczydlowski, E., O. Alvarez, C. Vergara, and R. Latorre. 1985. Effect of phospholipid surface charge on the conductance and gating of a Ca^{2+}-activated K^+ channel in planar lipid bilayers. *J. Membr. Biol*. 83:273–282.

Moczydlowski, E., and R. Latorre. 1983. Gating kinetics of Ca^{2+}-activated K^+ channels from rat muscle incorporated into planar lipid bilayers: evidence for two voltage-dependent Ca^{2+} binding reactions. *J. Gen. Physiol*. 82:511–542.

Monod, J., J. Wyman, and J.-P. Changeux. 1965. On the nature of allosteric transitions: a plausible model. *J. Mol. Biol*. 12:88–118.

Moss, B.L., S.D. Silberberg, C.M. Nimigean, and K.L. Magleby. 1999. Ca^{2+}-dependent gating mechanisms for dSlo, a large conductance Ca^{2+}-activated K^+ (BK) channel. *Biophys. J.* 76:3099–3117.

Munoz, A., L. Garcia, and A. Guerrero-Hernandez. 1998. In situ characterization of the Ca^{2+} sensitivity of large conductance Ca^{2+}-activated K^+ channels: implications for their use as near-membrane Ca^{2+} indicators in smooth muscle cells. *Biophys. J.* 75: 1774–1782.

Nimigean, C.M., and K.L. Magleby. 1999. The beta subunit increases the Ca^{2+} sensitivity of large conductance Ca^{2+}-activated potassium channels by retaining the gating in the bursting states. *J. Gen. Physiol*. 113:425–439.

Nonner, W., and B. Eisenberg. 1998. Ion permeation and glutamate residues linked by Poisson-Nernst-Plank theory in L-type calcium channels. *Biophys. J.* 75:1287–1305.

Oberhauser, A., O. Alvarez, and R. Latorre. 1988. Activation by divalent cations of a Ca^{2+}-activated K^+ channel from skeletal muscle membrane. *J. Gen. Physiol*. 92:67–86.

Pallanck, L., and B. Ganetzky. 1994. Cloning and characterization of human and mouse homologs of the *Drosophila* calcium-activated potassium channel gene, *slowpoke*. *Hum. Mol. Genet.* 3:1239–1243.

Pallotta, B.S. 1985. *N*-Bromoacetamide removes a calcium-dependent component of channel opening from calcium-activated potassium channels in rat skeletal muscle. *J. Gen. Physiol*. 86:601–611.

Petracchi, D., M. Barbi, M. Pellegrini, M. Pellegrino, and A. Simoni. 1991. Use of conditioned distributions in the analysis of ion channel recordings. *Eur. Biophys. J.* 20:31–39.

Reinhart, P.H., S. Chung, and I.B. Levitan. 1989. A family of calcium-dependent potassium channels from rat brain. *Neuron*. 2:1031–1041.

Rothberg, B.S., R.A. Bello, and K.L. Magleby. 1997. Two-dimensional components and hidden dependencies provide insight into ion channel gating mechanisms. *Biophys. J.* 72:2524–2544.

Rothberg, B.S., R.A. Bello, L. Song, and K.L. Magleby. 1996. High Ca^{2+} concentrations induce a low activity mode and reveal Ca^{2+}-independent long shut intervals in BK channels from rat muscle. *J. Physiol*. 493:673–689.

Rothberg, B.S., and K.L. Magleby. 1996. Gating of BK channels can be independent of calcium or voltage. *Soc. Neurosci. Abstr.* 22: 1443.

Rothberg, B.S., and K.L. Magleby. 1998. Kinetic structure of large-conductance Ca^{2+}-activated K^+ channels suggests that the gating includes transitions through intermediate or secondary states. A mechanism for flickers. *J. Gen. Physiol*. 111:751–780.

Rothberg, B.S., and K.L. Magleby. 1999. Voltage-dependent steps in the gating of single BK channels. *Biophys. J.* 76:A333.

Roux, B., and R. Sauve. 1985. A general solution for the time interval omission problem applied to single channel analysis. *Biophys. J.* 48:149–158.

Rudy, B. 1988. Diversity and ubiquity of K channels. *Neuroscience.* 25:729–749.

Schoppa, N.E., and F.J. Sigworth. 1998. Activation of *Shaker* potassium channels. III. An activation gating model for wild-type and V2 mutant channels. *J. Gen. Physiol*. 111:313–342.

Schreiber, M., and L. Salkoff. 1997. A novel calcium-sensing domain in the BK channel. *Biophys. J.* 73:1355–1363.

Schwarz, G. 1978. Estimating the dimension of a model. *Annals of Statistics.* 6:461–464.

Shen, K.-Z., A. Lagrutta, N.W. Davies, N.B. Standen, J.P. Adelman, and R.A. North. 1994. Tetraethylammonium block of *slowpoke* calcium-activated potassium channels expressed in *Xenopus* oocytes: evidence for tetrameric channel formation. *Pflügers Arch.* 426: 440–445.

Sigworth, F.J., and S.M. Sine. 1987. Data transformations for improved display and fitting of single-channel dwell time histograms. *Biophys. J.* 52:1047–1054.

Solaro, C.R., J.P. Ding, Z.W. Li, and C.J. Lingle. 1997. The cytosolic inactivation domains of BK channels in rat chromaffin cells do not behave like simple, open-channel blockers. *Biophys. J.* 73: 819–830.

Song, L., and K.L. Magleby. 1994. Testing for microscopic reversibility in the gating of maxi K^+ channels using two-dimensional dwell-time distributions. *Biophys. J.* 67:91–104.

Stefani, E., M. Ottolia, F. Noceti, R. Olcese, M. Wallner, R. Latorre, and L. Toro. 1997. Voltage-controlled gating in a large conductance Ca^{2+}-sensitive K^+ channel (hslo). *Proc. Natl. Acad. Sci. USA.* 94:5427–5431.

Talukder, G., and R.W. Aldrich. 1998. Intermediate states in the gating of single m*SLO* calcium activated potassium channels in the absence of calcium. *Biophys. J.* 74:A217. (Abstr.)

Tanaka, Y., P. Meera, M. Song, H.G. Knaus, and L. Toro. 1997. Molecular constituents of maxi K_{Ca} channels in human coronary smooth muscle: predominant alpha + beta subunit complexes. *J. Physiol*. 502:545–557.

Toro, L., M. Wallner, P. Meera, and Y. Tanaka. 1998. Maxi-K_{Ca}, a unique member of the voltage-gated K channel superfamily. *News Physiol. Sci.* 13:112–117.

Tseng-Crank, J., N. Godinot, T.E. Johansen, P.K. Ahring, D. Strobaek, R. Mertz, C.D. Foster, S.-P. Olsen, and P.H. Reinhart. 1996. Cloning, expression, and distribution of a Ca^{2+}-activated K^+ channel β-subunit from human brain. *Proc. Natl. Acad. Sci. USA.* 93:9200–9205.

Van der Kloot, W.G., and I. Cohen. 1979. Membrane surface poten-

tial changes may alter drug interactions: an example, acetylcholine and curare. *Science.* 203:1351–1353.

Vergara, C., and R. Latorre. 1983. Kinetics of Ca^{2+}-activated K^+ channels from rabbit muscle incorporated into planar lipid bilayers: evidence for a Ca^{2+} and Ba^{2+} blockade. *J. Gen. Physiol.* 82: 543–568.

Waller, M., P. Meera, and L. Toro. 1999. A novel beta subunit leads to inactivating maxi K currents. *Biophys. J.* 76:A267. (Abstr.)

Weiss, D.S., and K.L. Magleby. 1992. Voltage-dependent gating mechanism for single fast chloride channels from rat skeletal muscle. *J. Physiol.* 453:279–306.

Wong, B.S., H. Lecar, and M. Adler. 1982. Single calcium-dependent potassium channels in clonal anterior pituitary cells. *Biophys. J.* 39:313–317.

Wu, Y.-C., J.J. Art, M.B. Goodman, and R. Fettiplace. 1995. A kinetic description of the calcium-activated potassium channel and its application to electrical tuning of hair cells. *Prog. Biophys. Mol. Biol.* 63:131–158.

Zagotta, W.N., T. Hoshi, and R.W. Aldrich. 1994. *Shaker* potassium channel gating. III: Evaluation of kinetic models for activation. *J. Gen. Physiol.* 103:321–362.

Zheng, J., and F.J. Sigworth. 1998. Intermediate conductances during deactivation of heteromultimeric *Shaker* potassium channels. *J. Gen. Physiol.* 112:457–474.